JOURNAL OF GEOPHYSICAL RESEARCH, VOL. 112, A10221, doi:10.1029/2007JA012370, 2007

Equatorial electron beams and auroral structuring at Jupiter

Barry H. Mauk[1] and Joachim Saur[2]

Received 24 February 2007; revised 20 May 2007; accepted 11 July 2007; published 26 October 2007.

[1] It has been reported that low-altitude regions of downward electric current on auroral magnetic field lines are sites of dramatic upward magnetic field-aligned electron acceleration that generates intense magnetic field-aligned electron beams within Earth's equatorial middle magnetosphere. Field-aligned equatorial electron beams also are observed within Jupiter's middle magnetosphere. The mystery about these Jovian beams is that they are observed in a region thought to map to Jupiter's brightest aurora and on field lines that generally carry electric current away from Jupiter's atmosphere rather than toward the atmosphere as anticipated at Earth. Here we develop procedures for quantifying the character of the Jupiter electron beams (for example, how confined they are with respect to the magnetic field-aligned directions). We apply the procedures to the highest time resolution electron data available from the Galileo Energetic Particle Detector (EPD). We find that the Jupiter equatorial electron beams are spatially and/or temporally structured (down to <20 km at auroral altitudes, or less than several minutes), with regions of intense beams intermixed with regions absent of such beams. We suggest that, as with the situation at Earth, Jupiter's circuit of electric currents that supports its brightest aurora is structured, with regions of upward current intermixed with regions of downward current.

Citation: Mauk, B. H., and J. Saur (2007), Equatorial electron beams and auroral structuring at Jupiter, *J. Geophys. Res.*, *112*, A10221, doi:10.1029/2007JA012370.

1. Introduction

[2] The mapping of Earth's intense and dramatic auroral lights along magnetic fields into the distant magnetosphere has long been a highly contentious issue [e.g., *Meng et al.*, 1991]. Much effort has been expended, for example, in searching for unique signatures of auroral acceleration within the near-equatorial magnetosphere. The most successful of these efforts was achieved by *Klumpar et al.* [1988] as reinterpreted by *Carlson et al.* [1998]. *Klumpar et al.* [1988] discovered the occurrence of intense, bidirectional, magnetic field-aligned electron beams within the Earth's nightside, near-equatorial magnetosphere at radial distances of ~9–11 Earth radii (Figure 1, left). The authors hypothesized that these beams represent electrons that at one time, were accelerated toward the Earth at low altitudes in association with the generation of discrete aurora but later were released into the magnetosphere after the acceleration region shut down.

[3] *Carlson et al.* [1998] reinterpreted the *Klumpar et al.* [1988] observations on the basis of low-altitude observations close to the auroral acceleration region (Figure 2, from *Marklund et al.* [2001]). They observed electron beams similar to those observed by *Klumpar et al.* [1988] but in association with the regions of downward electric current that do not support intense discrete aurora. A defining signature of these beams, distinct from the downward accelerated electron beams associated with discrete aurora, is the character of the spectra of phase space density (PSD) plotted versus energy. The upward accelerated beams show broad spectra that vary monotonically with energy, having high-energy portions that extend in energy at least an order of magnitude higher than the energy that would be obtained by passing through the observed, roughly static downward electric field associated with the downward current regions [*Ergun et al.*, 1998]. Stochastic acceleration processes apparently play a major role in the generation of these beams in addition to the coherent acceleration arising from the static fields. In contrast, the PSD spectra of downward accelerated beams tend to retain the signatures of the coherent acceleration associated with static electric fields aligned with the magnetic field lines [*Carlson et al.*, 1998; *Ergun et al.*, 1998]. The equatorial electron beams apparently are a direct equatorial signature of low-altitude auroral acceleration processes. While they appear to represent regions of downward rather than upward current, experience at Earth suggests that downward auroral currents typically are closely adjacent to the regions of upward auroral currents associated with intense discrete aurora (Figure 2).

[4] A complicating factor is that more than one type of electron beam is observed within the Earth's equatorial magnetosphere. *McIlwain* [1975] discovered intense magnetic field-aligned electron beams in close association with

[1]Johns Hopkins University Applied Physics Laboratory, Laurel, Maryland, USA.
[2]Institut für Geophysik und Meteorologie, Universität zu Köln, Cologne, Germany.

0148-0227/07/2007JA012370$09.00

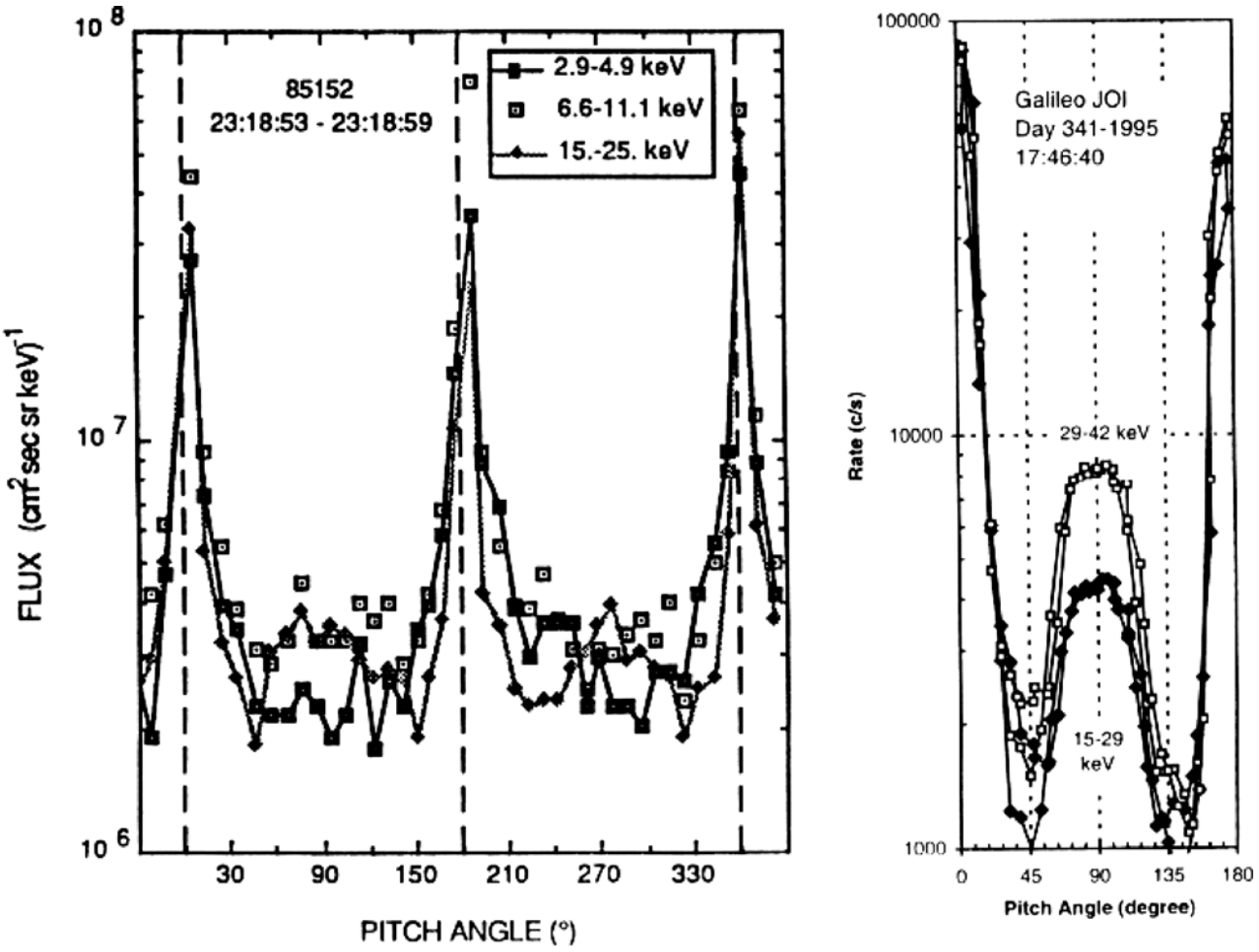

Figure 1. (left) Bidirectional electron beams observed near ~9 R_E, near the magnetic equator, and near midnight by the AMPTE CCE spacecraft as reported by *Klumpar et al.* [1988]. The pitch angle is the angle that the velocity vector of the sampled particles makes with respect to the local magnetic field vector. Angles shown as >180 degrees represent different portions of the sampling cycle and are to be interpreted with the values 360−180 degrees. (right) Similar beams observed in the plasma wake of Jupiter's moon Io near Jupiter's magnetic equator as discovered by *Williams et al.* [1996] and replotted by *Mauk et al.* [2001].

dynamic particle injections that occur concurrently with so-called magnetospheric substorms [see also *Mauk and Meng*, 1991]. These beams are transient rather than steady (several minutes), are observed closer to Earth (~6−7 Earth radii) than are the *Klumpar et al.* [1988] beams, show signatures of coherent acceleration with local maxima in the PSD spectra, and are associated with transient east-west magnetic field perturbations indicative of the occurrence of transient magnetic field-aligned currents (Figure 3, after *Mauk and Meng* [1991]). After the injection, these beams do evolve to broader distributions and without the peaked PSD versus energy feature. These beams may be associated with transient auroral emissions typically occurring equatorward of the main region of intense discrete aurora. Given multiple types of equatorial electron beams within the Earth's magnetosphere, care must be exercised in interpreting such beams observed at such extraterrestrial space environments as those of Jupiter and Saturn.

[5] Equatorial electron beams of varying intensities, in some cases better characterized as electron distributions with bidirectional enhancements in the magnetic field-aligned direction, have been reported within the broad magnetospheric environments of both Jupiter and Saturn. *Lanzerotti et al.* [1993] interpreted bidirectional electron beams observed at high latitudes with the Ulysses spacecraft in the context of auroral processes. *Frank and Paterson* [2000] reported the occurrence of such distributions within Jupiter's inner magnetosphere ($r < 10\ R_J$) and associated them with the radial interchange of small-scale magnetic flux tubes of hot and cold plasmas, respectively, as buoyancy forces drive the dense plasmas of Io's plasma torus outward. Such beams perhaps arise because of the coupling of Jupiter's ionosphere to its partially corotating magnetosphere. With this coupling are associated field-aligned electric currents that require electron acceleration in regions with sufficiently sparse charge-carrier density. Such distri-

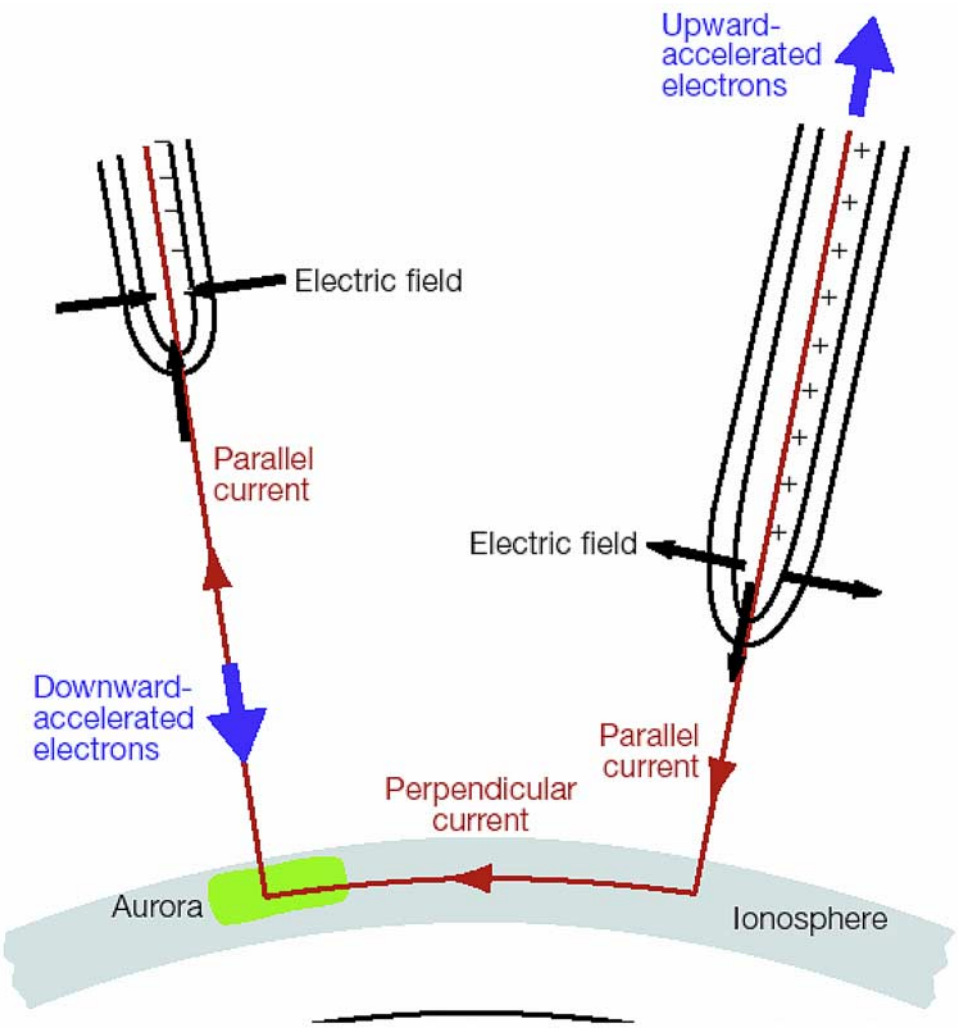

Figure 2. Schematic from *Marklund et al.* [2001], based on discoveries reported by *Carlson et al.* [1998], of the upward and downward field-aligned current regions of the aurora and their relationships to aurora emissions and upward-accelerated electron beams. Wave turbulence, over and above steady electrostatic forces, likely contributes at least to the upward electron accelerations [*Ergun et al.*, 1998]. Copyright by the Nature Publishing Group.

butions also are observed in Jupiter's middle magnetosphere (from 15 to >30 R_J) [*Bhattacharya et al.*, 2001; *Frank and Paterson*, 2002, 2004; *Tomás et al.*, 2004a, 2004b] over a broad radial range that includes the region that maps magnetically to Jupiter's most intense aurora.

[6] Similar electron beams also are observed in the vicinity of Jupiter's moon Io. *Williams et al.* [1996] discovered such beams in the plasma wake of Io with peak-to-valley ratios quite comparable to those observed at Earth (Figure 1, right). They later were observed over the poles of Io [*Williams et al.*, 1999] and at much lower energies [*Frank and Paterson*, 1999]. By combining both low- and high-energy components to reveal a broad, power-law shape to the intensity versus energy spectrum from <0.2 to ~200 keV, *Mauk et al.* [2001] hypothesized that these beams can be interpreted in the context of the *Carlson et al.* [1998] picture (Figure 2), with the observed near-Io beams associated with the downward (with respect to Jupiter) electric current regions. With this interpretation, the auroral emissions at Io's magnetic footprint are generated by downward accelerated, low-altitude electron beams that are not observed near Io.

[7] Finally, the occurrences of such beams at Saturn recently were reported [*Saur et al.*, 2006] and were attributed to auroral processes. Because of the ubiquitous nature of equatorial electron beams at Earth, Jupiter, and Saturn, these authors argue that the upward acceleration of electrons is a universal aspect of discrete auroral processes that otherwise requires only downward acceleration to explain the auroral emissions. Downward acceleration of electrons arises naturally from the magnetic field-aligned electric fields that regulate the flow of magnetic field-aligned currents in an environment that has insufficient charge carriers. The upward electron acceleration is far less understood and studied [*Temerin and Carlson*, 1998; *Anderson et al.*, 2002]. The acceleration of particles often is related

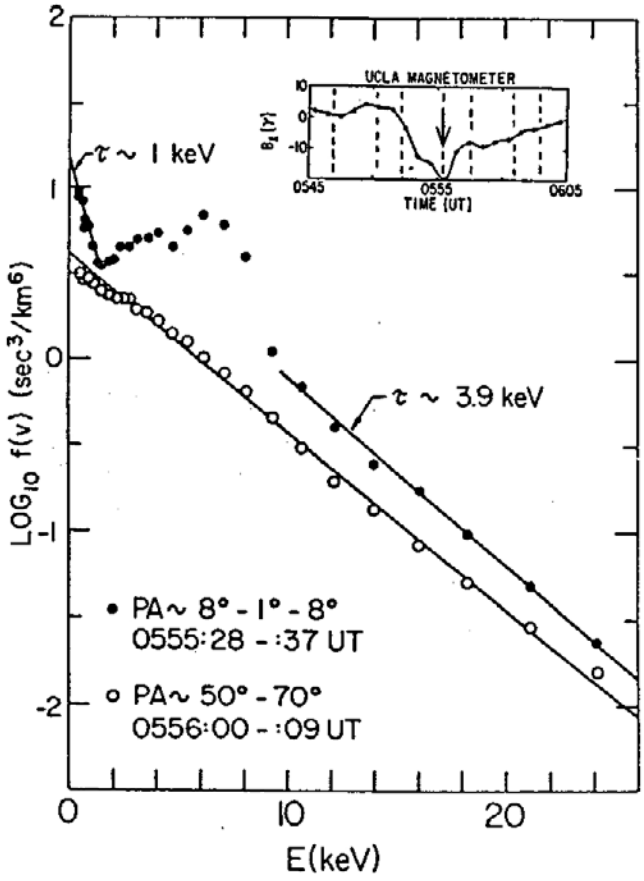

Figure 3. Equatorial magnetic field-aligned electron beams discovered by *McIlwain* [1975] within the Earth's geosynchronous magnetosphere (~6.7 R_E) near midnight. Such beams with phase-space-density distributions (directional f[**v**] plotted versus speed |**v**| or energy E) with positive slopes are observed in close association with so-called substorm injections and magnetic signatures of magnetic field-aligned electric currents (see inserted magnetic field signature). This figure represents a replotting of the *McIlwain* [1975] data as presented by *Fritz et al.* [1977] and *Mauk and Meng* [1991]. The parameter PA is the pitch angle, which represents the angle between the velocity vector of the particles and the local magnetic field direction. Figure publicly released by *Fritz et al.* [1977].

either to electrostatic potential structures or to regions of strong Alfvén wave activity [e.g., *Su et al.*, 2003].

[8] The mystery that we explore in this paper arises from the work of *Tomás et al.* [2004a, 2004b]. These authors found that not only do the bidirectional magnetic field-aligned electron enhancements occur within the middle Jovian magnetosphere but they also are continually present over a broad region that extends from an inner boundary somewhere between 10 and 17 R_J and an outer boundary that can extend beyond 30 R_J (Figure 4). Yet the outer portions of this radial range include the region that is thought to be dominated by upward field-aligned currents that, in turn, drive Jupiter's bright ring of discrete auroral emissions (Figure 5, after *Hill* [1979, 2001], *Vasyliunas* [1983], *Cowley and Bunce* [2001]). On the basis of our concepts derived from Earth observations, the equatorial electron beams should be associated with downward field-aligned currents, not upward field-aligned currents. However, these are steady-state approaches, and they divide Jupiter's magnetosphere into an inner/middle magnetosphere in which the electric current is going upward only and an outer part in which the current is in the reverse direction. Other approaches to an acceleration mechanism for the Jupiter's main auroral oval assume a more dynamic Jovian magnetosphere. For example, *Saur et al.* [2006] argue that turbulent Alfvén waves with associated field-aligned electric currents are dissipated near the high latitudes to turn the wave energy into particle acceleration and heating.

[9] A possible resolution of the mystery of the location of the *Tomás et al.* [2004a, 2004b] electron beams with respect to Jupiter's aurora might be that the beams are caused by processes other than those anticipated by Earth's auroral processes. In addition to very general suggestions involving wave acceleration that might occur preferentially in the field-aligned direction, both *Bhattacharya et al.* [2001] and *Tomás et al.* [2004a, 2004b] suggest that the process discussed by *Nishida* [1976] might play a role. A crucial aspect of this model is the assumption that electrons may be transported across magnetic field lines very close to the planet at high latitudes more easily than they can be transported near the equator. However, no convincing mechanism has ever been proposed to explain why the transport would be faster where the magnetic field strength is high than it is where the magnetic field strength is weak. Note in particular that for a dipolar configuration, the distance between two radially displaced field lines, when measured in units of the charged particle gyroradius of a given species and energy, in fact is substantially larger at low altitudes than it is at high altitudes (by roughly a factor of the magnetospheric distance parameter L). *Frank and Paterson* [2002, 2004] suggest that the observed equatorial electron beams are generated within the auroral emission region and are a direct signature of the processes that generate the auroral emissions. This proposal has the Occam's Razor advantage of unifying disparate observations with a single (but not developed or characterized) mechanism, but it has the disadvantage of being distinct from the auroral processes observed to be occurring at Earth. One can envision a heating mechanism that sends energized electrons simultaneously upward and downward from the acceleration site. However, before forcing an explanation that is contrary to Earth-derived expectations, we examine more carefully those expectations.

[10] It is our hypothesis that electrons beams are generated in Jupiter's broad middle magnetosphere in regions of downward field-aligned currents just like they are at Earth. We propose that the reason the beams are observed in the broad regions of upward currents is because the current system is highly structured with regions of downward current closely adjacent to regions of upward current. In testing this hypothesis, there are several aspects of the beams that we consider. First, we look at the electron angular distributions with higher time and angular resolution than were used by *Tomás et al.* [2004a, 2004b] in establishing the more global characteristics of these distributions. This requirement is a challenge because, as we discuss, high-resolution data from the ailing Galileo space-

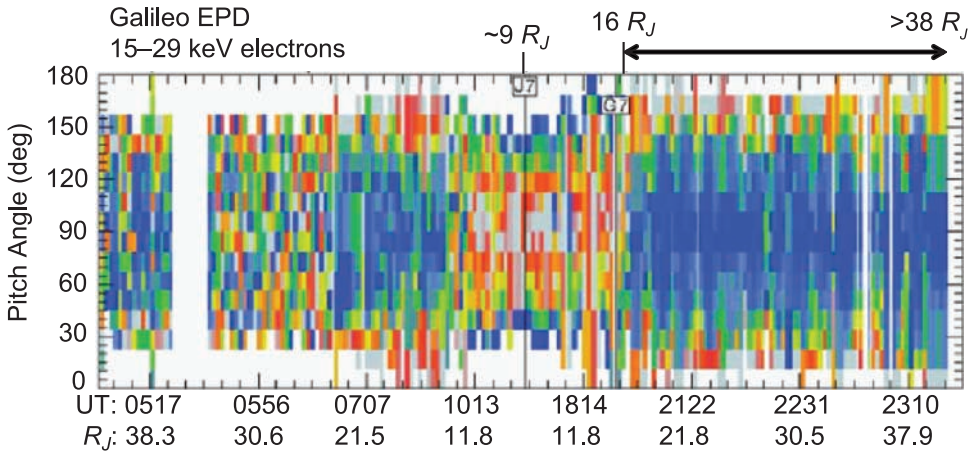

Figure 4. Relative intensity versus pitch angle versus time and position for 15- to 29-keV electron data as generated and reported by *Tomás et al.* [2004a, 2004b] using data from the Galileo EPD instrument at Jupiter. The pitch angle is the angle that the particle velocity vectors make with the local magnetic field direction. To obtain greater contrast in the display, the pitch-angle distributions for each record (vertical lines) are renormalized to a maximum of 1 and a minimum of 0 on a record-by-record basis. The colors represent relative normalized intensities in the following descending order: off-white, orange, red, light green, dark green, light blue, and dark blue, with off-white representing values near 1 and dark blue representing values near 0.

craft is only sparsely available. Second, we must establish some criterion for deciding what is a beam and what is not a beam. A major accomplishment of the present work, we believe, is the establishment of a technique for quantitatively evaluating the beam-like characteristics of the electron distributions. Finally, we must address the relationship between the beams and possible signatures of magnetic field-aligned currents.

[11] We begin in the sections to follow by first documenting the available Galileo Energetic Particle Detector (EPD) high-resolution data. We describe the technique for quantitatively evaluating the character of the electron beams. We then use the technique on the high time-resolution data that are available within our region of interest. We finally examine magnetic field short-scale structures, transients, and turbulent fluctuations within the regions that show the electron beaming. We close with a discussion of the implications of our findings on the processes of aurora at Jupiter and how they compare to the processes found at Earth.

2. Galileo Electron Data

[12] The Galileo EPD instrument, described by *Williams et al.* [1992], obtained the data analyzed here. The low-energy electron channels from the Low-Energy Magnetospheric Measurements System (LEMMS) are used, covering the energies from 15 to 884 keV in eight channels (E0–E3, F0–F3). Because they deliver the most-refined angular resolution (64 sectors per spacecraft spin compared to 32 for the other channels), the two lowest-energy channels E0 (15–29 keV) and E1 (29–42 keV) are the key channels used here. LEMMS uses a stepping motor to position the ~15-degree full-width view cone of the electron sensor into one of eight spacecraft elevation angles (elevation angles 0, 30, 60, 90, 120, 150, and 180 degrees with respect to the spacecraft spin axis plus one position viewing a 2-mm aluminum background shield). In each of these stepping positions, spacecraft rotation allows sampling of up to 64 different azimuth angles, yielding roughly 4π steradian angular coverage. The sensor is aligned roughly with one or the other end of the magnetic field vector during one or two of the motor stepping periods, which yields one or two pitch-angle distributions (with sample times of 20 s) obtained every 160 s. One bidirectional distribution (parallel and antiparallel to the magnetic field) is obtained every 160 s when the magnetic field is normal to the spin axis, and two monodirectional distributions are obtained every 160 s

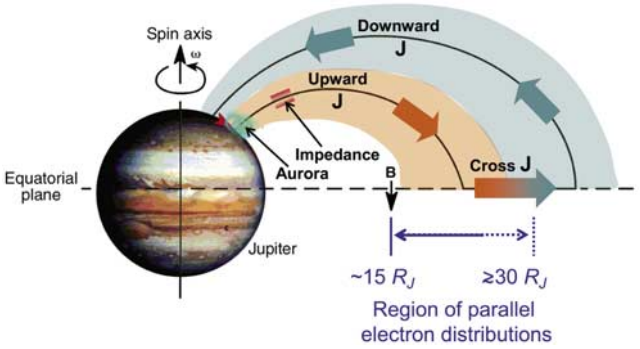

Figure 5. Schematic of the relationship between observed equatorial electron field-aligned enhancements reported by *Tomás et al.* [2004a, 2004b] and the circuit of electric currents that connects Jupiter's middle magnetosphere to the auroral ionosphere. The auroral circuit figure is based on concepts of *Hill* [1979] and *Vasyliunas* [1983] as replotted by *Mauk et al.* [2002]. It is understood that the shape of the field lines in the actual Jovian system are substantially stretched away from the dipolar configuration.

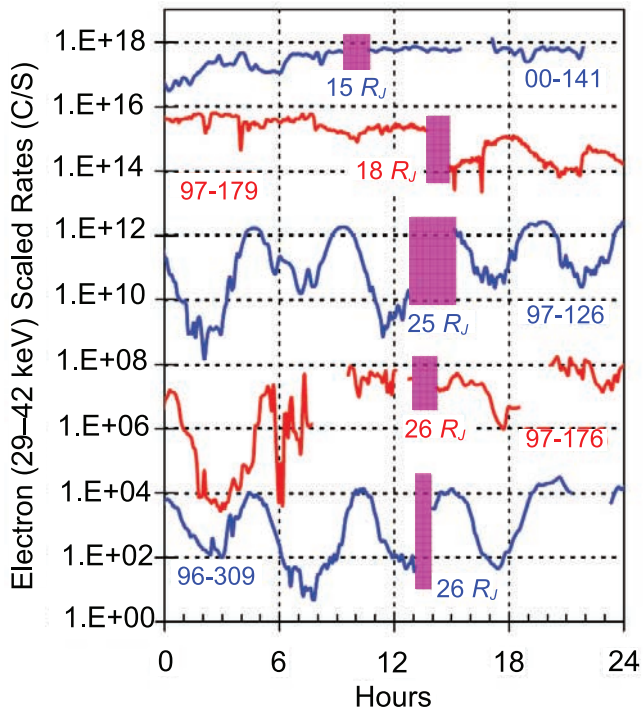

Figure 6. Twenty-four-hour context plots of electron relative intensities for each of the five high-resolution sampling periods analyzed in this report. The violet bars show the periods of high-resolution sampling. The plots are vertically displaced with arbitrary multipliers to separate the plots. Each plot is annotated with the two-digit year and three-digit day-of-year (e.g., 97–126 for day 126, 1997), and the approximate radial distance to the center of Jupiter at the position of the high-resolution sampling.

when the magnetic field has as substantial component along the spin axis.

[13] Because the high-gain antenna on the Galileo spacecraft failed to deploy, the EPD data rate typically was 5 bits per second (and sometimes twice that value) during the so-called "real-time" periods when the data were beamed directly to Earth while the data were being taken. During these periods, covering most of the >30 orbits that cut radially through Jupiter's space environment, the EPD data were averaged extensively to record just four spin sectors (down from 32–64) together with the seven step positions. Also, typically a total of 11 minutes was required to obtain one complete distribution. Sophisticated data analysis techniques were used by *Tomás et al.* [2004a, 2004b] on these data to discover the persistence of the bidirectional, field-aligned enhancements in the electron distributions in Jupiter's middle magnetosphere (Figure 4).

[14] Very occasionally, the Galileo spacecraft utilized a so-called "record mode," which allowed full-resolution data to be obtained from the instruments. For the region of interest here, the radial range of 15–35 R_J, there are five record mode periods available with the information that we need for our analyses. In Figure 6, these periods of time are shown as violet bars placed in the context of 24-hour plots of the real-time data. Some of these context plots reveal the roughly 5-hour periodicity associated with Jupiter's rotation combined with the 10-degree magnetic axis tilt, which causes the spacecraft to dip into and out of the plasma sheet particles that populate the Jupiter magnetodisc. The context plots also show other intervals in which the magnetospheric conditions were too highly disturbed to cleanly reveal the spin modulation (day 176, 1997) or the spacecraft was relatively close to Jupiter where the thickness of the plasma sheet is too large to reveal a strong spin modulation (day 141, 2000). A complicating issue is the fact that the record mode periods often were used to capture high-resolution data during encounters with Jovian satellites. Thus care must be exercised to make sure that the effects of the near-satellite environments are separated from the environmental effects of Jupiter's middle magnetosphere.

3. What Constitutes a Beam?

[15] There is no uniform terminology for electron distributions that show magnetic field-aligned bidirectional enhancements. They have been called "beams," "scattered beams," "bidirectional enhancements," "cigar distributions," and "butterfly distributions"; the latter terminology

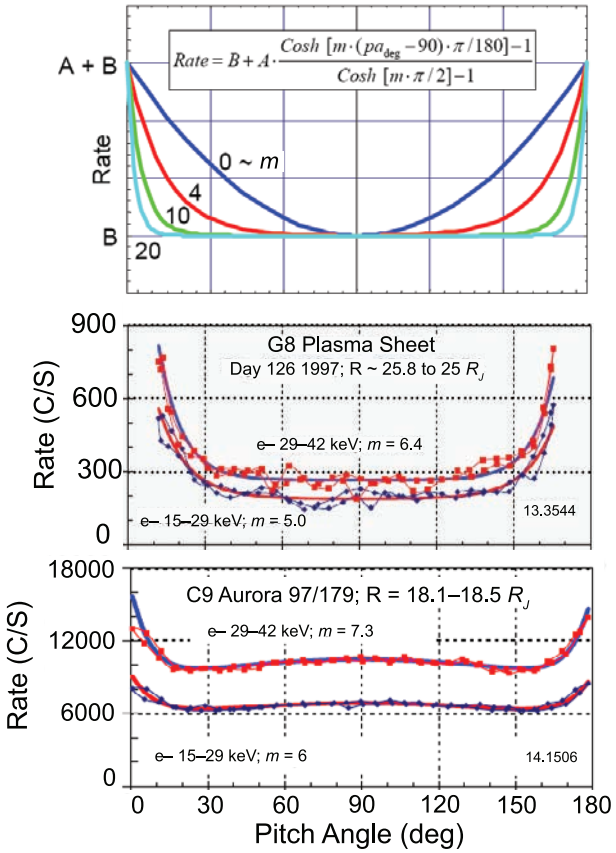

Figure 7. (top) Plot of the pitch-angle distribution-fitting function showing that the parameter m controls how closely aligned the distribution is to the magnetic field direction. (middle) Example of electron beam distributions fit with our fitting function. (bottom) Example of a pitch-angle distribution with a local maximum at 90-degree pitch angle. For such cases the fitting function is modified by replacing the parameter B with a two-parameter parabolic function.

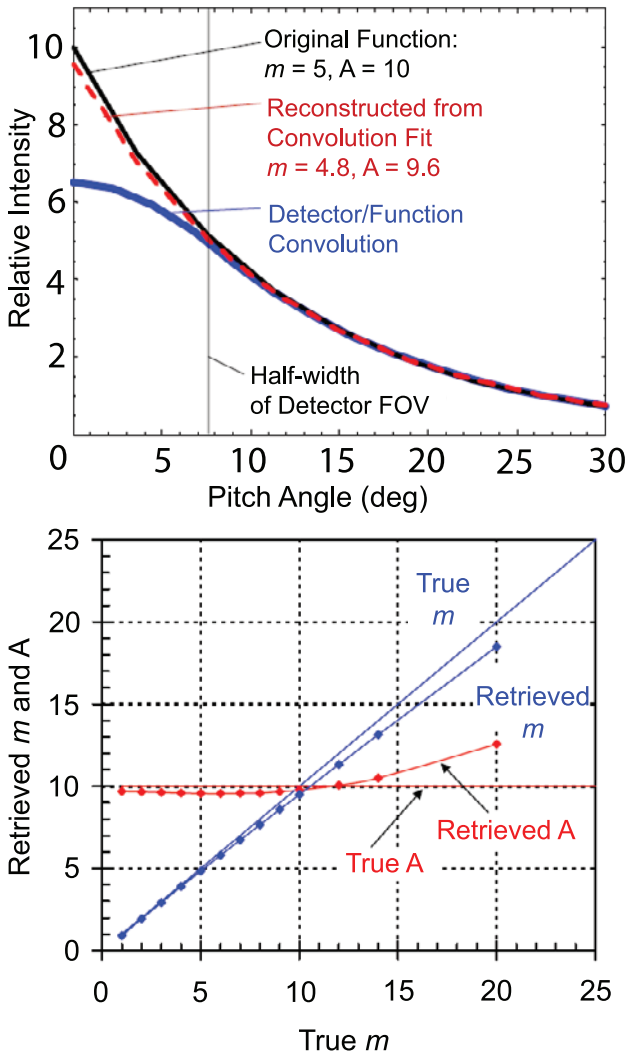

Figure 8. (top) Comparison of an initial ideal pitch-angle distribution (black) with the result of convoluting that distribution with the ~15-degree full-width view cone of the Galileo EPD instrument (blue, the "measured" distribution) and finally with the "deconvolution" (red) of the measured distribution with the view cone by utilizing our simplified deconvolution procedure. Our procedure consists of fitting that portion of the measured distribution that resides at angles ≥15/2 degrees. (bottom) Test of the success of our deconvolution procedure in retrieving the true parameters of ideal test distributions for a broad range of the parameter *m*.

applies when the distribution, as a function of angle away from the direction normal to the field, shows a decrease after increasing as the sensor approaches the field-aligned direction. *Frank and Paterson* [2002] make a qualitative distinction between what they call field-aligned beams and scattered beams. Here we develop a quantitative tool for assessing what constitutes a beam and what constitutes a bidirectional enhancement, cigar distributions, or a scattered beam. The tool involves fitting the distributions with a parametric functional form in which a single parameter quantifies the "beam-ness" of the distribution.

[16] Our functional form uses the hyperbolic cosine with the form:

$$Rate = B + A \cdot \frac{Cosh\left[m \cdot \left(pa_{\deg} - 90\right) \cdot \pi/180\right] - 1}{Cosh[m \cdot \pi/2] - 1}, \quad (1)$$

where $pa_{\deg}$ is the pitch angle, which is the angle that the velocity vector of the particles makes with the local magnetic field vector, and A, B, and m are our free-fitting parameters. This function is plotted in Figure 7a, which clearly shows that the parameter m characterizes how closely the electron beam resides to the magnetic field direction. Note that as $m \rightarrow 0$, equation (1) reduces to a perfect parabola. The parameter m can be characterized in terms of the one-half width of the pitch-angle distribution away from $pa = 0$ at the half maximum value (HWHM, evaluated at the rate value of $B + A/2$). The following list of pairs, showing [m, PA_{HWHM} in degrees], provides examples of that relationship: [~0, 26.3], [1, 23.4], [3, 12.9], [4, 9.9], [5, 7.9], [10, 4.0], [15, 2.6], [20, 2.0], and [25, 1.6]. When the observed distribution has the general form of equation (1), a simple least-squares minimization that optimizes the three parameters A, B, and m is used to fit the distributions. Figure 7b shows a sample fit.

[17] There are times when the distribution shows a local maximum at a 90-degree pitch angle, revealing a traditional trapping distribution. In such cases we replace B in equation (1) with a parabolic form: $B - C(pa_{\text{radian}} - \pi/2)^2$, where our fitting parameters now are A, B, C, and m. A parabolic form is chosen because it has no singularities near the directions aligned with the magnetic field that would disrupt the characterization of the beams (contrary to the often-utilized $\sin^n(pa)$ distribution) and because it forms a nearly linear extrapolation into the small pitch-angle regions, forming a stable baseline against which to characterize the nearly aligned beams. Because of coupling between parameters in the minimization process (potentially yielding nonunique solutions), we first fit the near 90-degree regions with the parabolic form (finding the parameters B and C) and then fit the entire distribution by optimizing the parameters A and m. This procedure is chosen, rather than inventing another parametric form for these situations, to preserve the uniqueness of the parameter m as a measure of the beam-ness of the field-aligned distributions. The procedure is found to be robust to variations in the range of pitch angles chosen around the 90-degree position for the initial fit and also robust to other kinds of perturbations to the initial conditions. Figure 7c show a sample of this kind of fit.

[18] A complication is the finite size, 15 degrees full-width, of the electron detector view cone. Figure 8 upper shows the consequences (blue line) of the convolution of the view cone with the "true" pitch-angle distribution (black line). The intensities closest to the direction of the magnetic field are substantially degraded from the true intensities. We have found that rather than performing a comprehensive and complicated deconvolution, we can retrieve nearly the original distribution simply by fitting

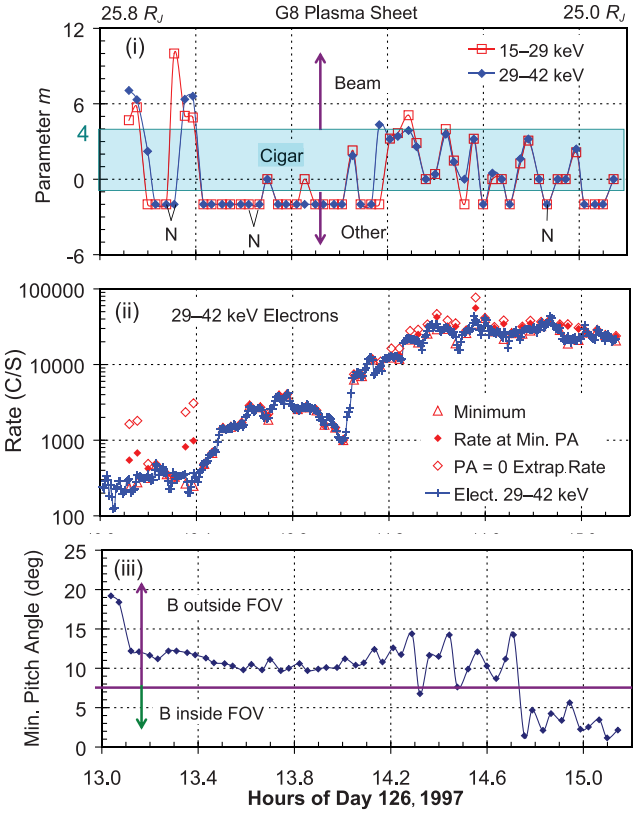

Figure 9a. Results of fitting the pitch-angle distributions for a high-resolution sample period designated as the G8 Plasma Sheet period. (top) Time profile of the m parameter of our fits for the two lowest-energy electron channels sampled by Galileo EPD. Isotropic distributions (see text for definition) are assign the parameter $m = -2$. Distributions with $m \geq 4$ are designated beams, and those with $4 \leq m \leq 0$ are designated as cigar distributions. (middle) Counting rates for 29- to 42-keV electrons. The different colors represent angle-averaged rates for every instrument stepping cycle (blue; every 20 s), rates actually measured at the minimum pitch angle sampled (solid red diamonds), rates obtained by extrapolating the fit functions to 0-degree pitch angle (open red diamonds), and the minimum rate measured at any pitch angle (open red triangle). (bottom) Plot of the minimum pitch angle sampled by Galileo EPD for those distributions that are fitted.

only that portion of the pitch-angle distribution that resides at center angles greater than 15/2 degrees away for the aligned directions (Figure 8 upper, dashed red line). Figure 8 lower tests the retrieval of the values of A and m, plotted as a function of m. The signal is lost for large values of m by using this procedure, with the consequence being that our statistical test (described in the next paragraph) is more difficult to pass. On the other hand, the <7.5-degree portion of the signal is not useful for constraining the value of m when m is very large. Other procedures might retain more solutions but with the consequence of very uncertain answers for those saved solutions.

[19] A final critical element to our analysis is the error analysis that must be used to determine whether the beam is statistically significant. In our analysis, a beam is considered real if those data points that are higher than the distribution minimum plus 90% of the difference between the minimum and the maximum are at least three standard deviations above the minimum value. The standard deviation is derived in the usual way, based on the differences between the functional fit and the 64 data points that comprise the measured angular distributions. This procedure has the quality of being generally consistent with the authors' subjective judgments of which beams seem to be real and which beams are suspicious and possibly the result of fluctuations. When a distribution failed the statistical test, it was assigned the status of "other," which generally means either isotropic or trapped (peaking only near 90 degrees) distributions. In some instances, in the plots presented in the next section, an "N" (for noisy) is positioned close to some data points that failed our statistical test but where beam-like structures subjectively were sensed by the authors. It should be noted that a feature that fails a statistical test when sampled over 20 s (our sample period) may represent a relatively robust feature when sampled over 11 min (the sample period used by *Tomás et al.* [2004a, 2004b]). Therefore some regions in the present analysis that are labeled isotropic may represent cigar-like distributions in the analysis of these latter authors.

4. Analysis of Record Mode Data

4.1. Orbit G8 Plasma Sheet Encounter, Day 126, 1997 (25.4 R_J)

[20] A sample of our standard result plots is shown in Figure 9a for the day 126, 1997, record mode period labeled the "G8 Plasma Sheet Encounter," where the 8 represents the Galileo orbit number and the G represents the icy moon (Ganymede) that was targeted during this orbit. The data shown in Figure 9a were taken far away from Ganymede. This record mode period was planned by the Galileo Project for the purposes of characterizing Jupiter's plasma sheet populations. There are no icy moon encounters during the displayed period of time. Figure 9a (top) shows the m values, derived from our fits, for the two low-energy electron channels: 15–29 keV and 29–42 keV. On this display and others, we have made the arbitrary and subjective decision that beams are defined as having $m \geq 4$ based on the impression that, with $m \geq 4$, there is a clean separation between the field-aligned enhancement feature and the character of the distributions near the 90-degree pitch angle. Cigar distributions (read also scattered beams) have $0 \leq m < 4$. This region in Figure 9a (top) is highlighted with blue shading. Isotropic distributions are assigned the value $m = -2$ for clarity on the plot. Note that this assignment is an arbitrary convention because all valid solutions have $m \geq 0$.

[21] Figure 9a (middle) shows channel counting rates for the 29–42 keV channel. Blue connected crosses represent spin-averaged rates for all stepping sectors. Solid red diamonds are the rates at the minimum pitch angle viewed by the sensor only for those stepping sectors that yield relatively aligned pitch-angle sampling. Open red diamonds are the rates for 0-degree pitch angle obtained by extrapolating with the fitted function (representing, for example, the number $A + B$ for the equation (1) function form). This

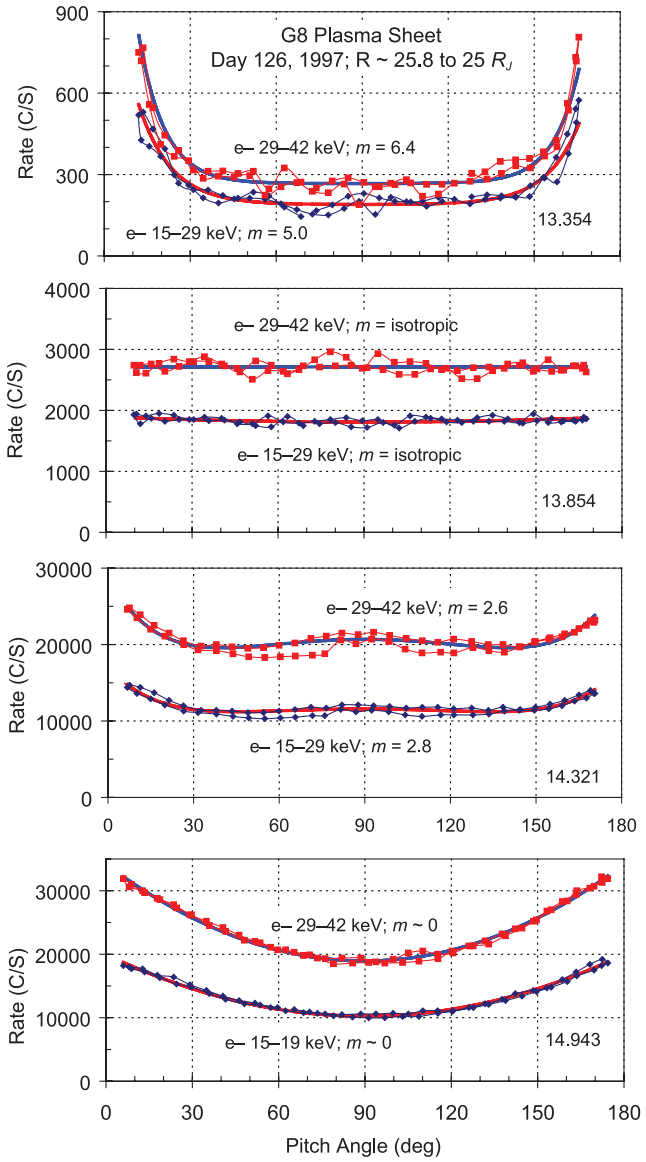

Figure 9b. Sample electron pitch-angle distributions and fits selected from the time period represented in Figure 9a.

value is what an ideal detector, with delta-function angular response, would see if it looked exactly along the magnetic field line. The open red triangle represents the minimum rate observed and is included for those situations where there is a local maximum at 90 degrees.

[22] Figure 9a (bottom) shows the minimum pitch angle viewed by the center of the detector view cone. A horizontal line is placed at ~15/2 degrees as a demarcation between the situation when the magnetic field line resides within the view cone at the time of the minimum pitch-angle sample and when the magnetic field stays outside of the view cone. When the magnetic field stays outside of the view cone, beams with very high *m* values may not be visible.

[23] We preliminarily conclude from Figure 9a that there is a high degree of structuring in the beaming characteristic of the electron distributions. Two brief periods of robust beaming are observed at the very beginning of the period of

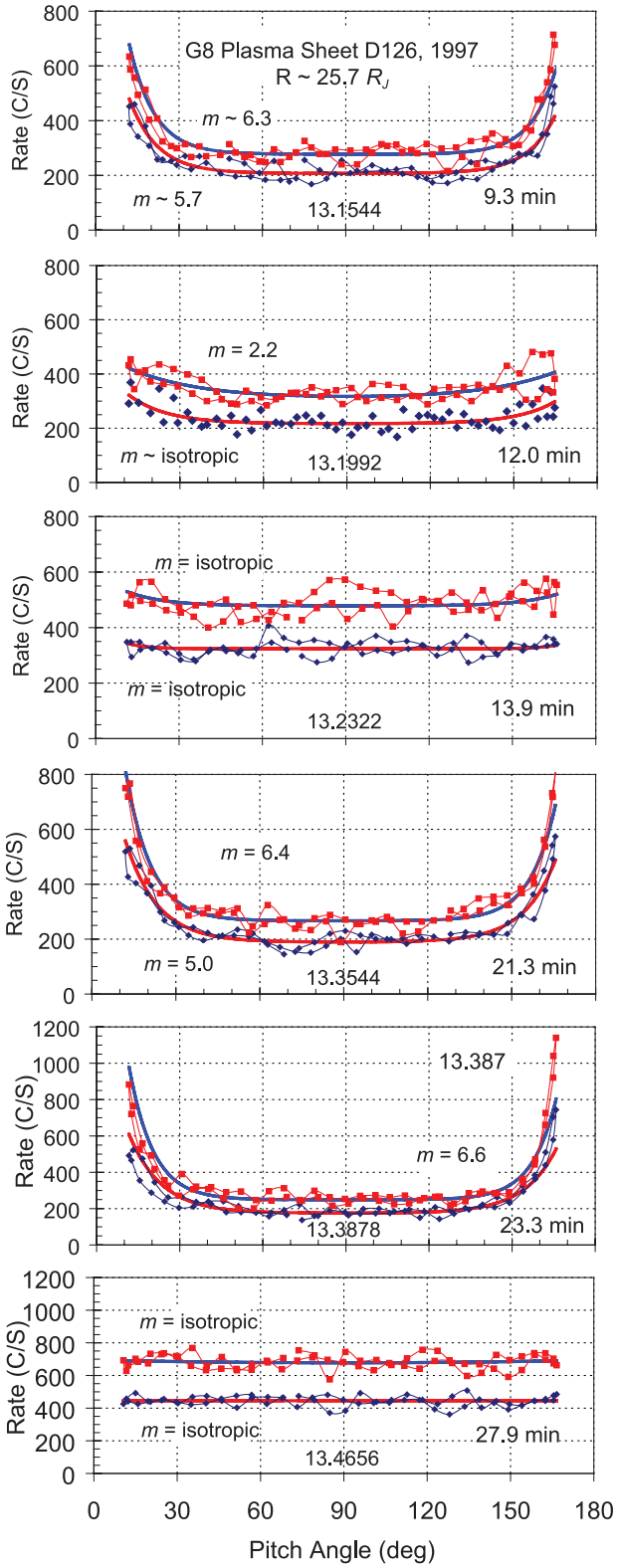

Figure 9c. A time series of electron pitch-angle distributions sampled at the very beginning of the time period shown in Figure 9a. The fractional hour of the day for each panel is given at the bottom of the plot (e.g., 13.1544 for the first panel). The number of minutes into the hour (hour 13) is shown in the lower right-hand corner of each plot (e.g., 9.3 min for the first panel).

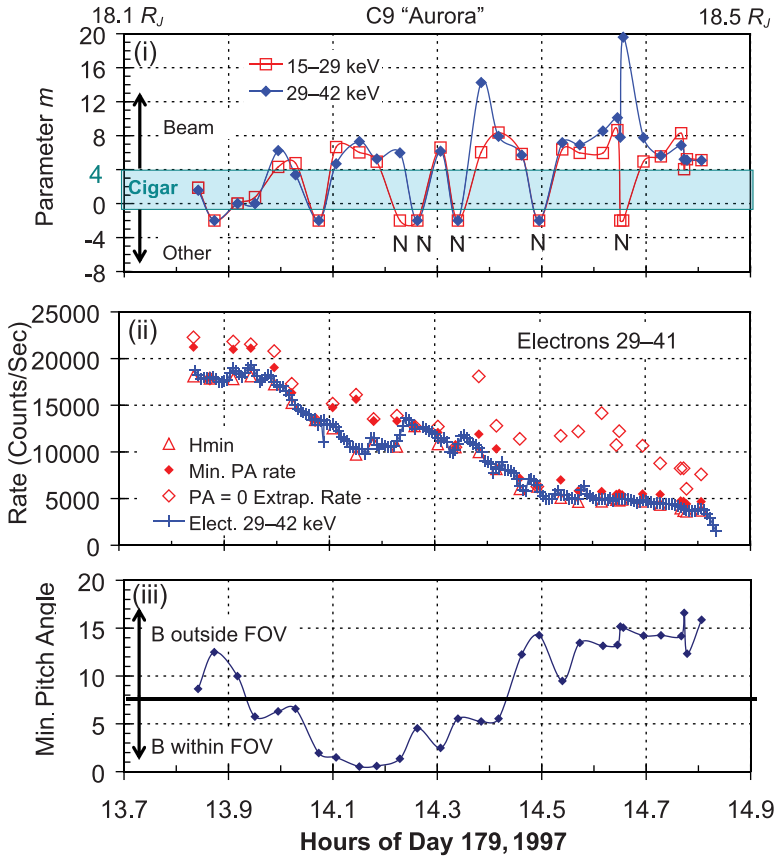

Figure 10a. Results of fitting the pitch-angle distributions for a high-resolution sample period designated as the C9 Aurora period. The description is the same as in the Figure 9a legend.

interest (where the average electron intensities are low). Assuming that these features are spatial in character, the spatial scale of these beaming periods at auroral altitudes may be estimated by using the constancy of magnetic flux $\mathbf{\Phi} = \mathbf{B} \cdot \mathbf{A}$, where **B** is magnetic field strength and **A** is flux shell cross-sectional area with direction normal to the area. By combining the observed temporal scale with the spacecraft speed, one can estimate auroral altitude scales on the order of ~15 km. If the features are temporal in character, then the temporal scale is represented by the time over which the beams were observed, 3–6 min. Elsewhere such beaming is observed only marginally, the distributions more often representing cigar or isotropic configurations. A variety of angular distribution types are observed through the period displayed. Figure 9b, a sampling of different distribution types within the Figure 9a period, shows that the diversity of distribution types is qualitative and not just quantitative. We observe true beaming (Figure 9b, top), truly isotropic distributions (Figure 9b, middle), and truly cigar distributions (Figure 9b, bottom; with the field-aligned enhancement spreading across the entire pitch-angle range).

[24] Figure 9c shows a time series of distributions that demonstrates that the temporal or spatially varying nature of the beams at the beginning of the Figure 9a time period is quite real and again not an artifact of the fitting procedures.

4.2. Orbit C9 Aurora, Day 179, 1997 (18.3 R_J)

[25] Our second record mode period of time (Figure 10a; Orbit 9, target Callisto and at ~18.3 R_J) was planned by the Galileo Project to possibly characterize the regions that might map to Jupiter's auroral regions on the edge of the nominal plasma sheet. Again, there were no icy moon encounters during this period. Here we begin with a 15-min period with considerable diversity in the electron distribution types (cigars, truly isotropic, and beaming) followed by a roughly 40-min period of relatively steady beaming. We note that following the hour 14.1, there is apparent structuring, but the numerous Ns labeling the isotropic distributions that follow that time are used by the authors of this paper to declare that the jumping up and down of the *m* parameter results from the fact that the beams reside fairly close the detection threshold, causing the distributions sometimes to fail our statistical test. If we were to remove the points labeled N from consideration, the beaming would appear to be relatively steady for the 40-min period. Figure 10b shows again that the diversity of distributions types suggested by Figure 10a is real. Figure 10b (bottom) also shows how weak some of the beams are relative to the background intensities and why they sometimes fail our statistical test.

[26] This Figure 10 sampling of electron distributions near 18 R_J, as with our previous period near 25 R_J, again

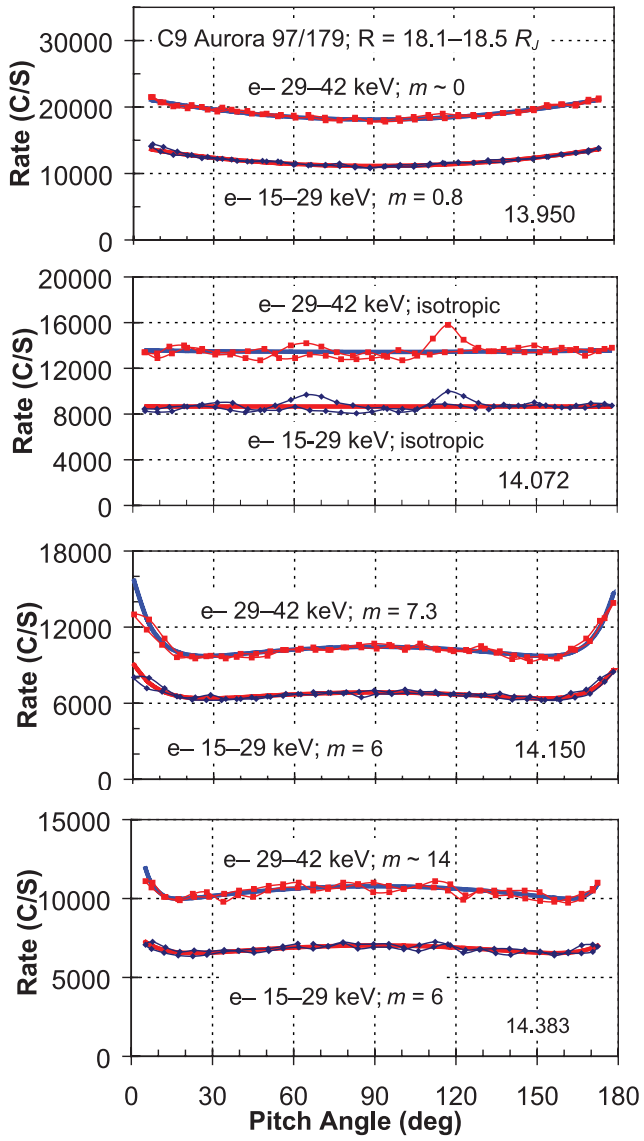

Figure 10b. Sample electron pitch-angle distributions and fits selected from the time period represented in Figure 10a.

reveals that the electron distributions at any one position are diverse and that the beaming characteristic is structured. Here, though, we may have a period of relatively constant beaming that lasts 40 min or a radial distance of ~0.3 R_J. With the constancy of $\mathbf{B} \cdot \mathbf{A}$, where $\mathbf{B}$ is magnetic field strength and $\mathbf{A}$ is flux shell cross-sectional area, such a distance translates into ~200 km within the auroral ionosphere, assuming that the event represents spatial rather than temporal structuring.

4.3. Orbit G28 Encounter, Day 141, 2000 (15 R_J)

[27] Still closer to Jupiter (~15 R_J from Jupiter's center), we have the Ganymede encounter record mode period (Figure 11a) that occurred during Galileo orbit 28 on day 141, 2000. As with all of the remaining periods, here we face the issue of separating the effects of the icy moon environments (in this case that of Ganymede) and the broader environment of Jupiter. The radial distance to Ganymede's center (in units of Ganymede's radius) are shown in the upper portion of Figure 11a (bottom), and a clear signature of Ganymede's presence is shown in a rate versus time profile in Figure 11a (middle). While Galileo passes Ganymede on the upstream side with respect to the flow of Jupiter's plasmas, a strong signature of Ganymede is observed as a result of Galileo passing onto closed magnetic field lines that are connected to Ganymede on both of their ends. Pitch-angle fits are not provided for the near-Ganymede distributions, all within the bounds of Ganymede's "magnetopause" as defined by *Williams* [2001]. The distributions observed on closed field lines show a strong trapping distribution with no signatures of field-aligned beaming. A few other distributions, still within the bounds of the magnetopause, show a lack of coherence over the 20 s needed to sample them.

[28] The visual impression of Figure 11a, and the identification of the limits of Ganymede's influence by *Williams* [2001], leads us to the belief that the field-aligned enhancements in the regions away from Ganymede in Figure 11a are a property of Jupiter's environment as distinct from the environment of Ganymede. Here the distributions reside close to the boundary of what we describe as beams and what we describe as cigar distributions, or scattered beams (see examples in Figure 11b). Interpolating through the Ganymede encounter region, we see that the beaming characteristics are relatively steady for a period of again ~40 min (translating here to 300-km sizes within the ionosphere). The variations in the postencounter regions appear to be real features of Jupiter's environment, and so even in this region near the inner boundary of where field-aligned enhanced distributions prevail [*Tomás et al.*, 2004a, 2004b], the distributions show some spatial or temporal structuring.

4.4. Two Callisto Encounters

[29] The problem of separating icy moon environments from the broader environment of Jupiter is a greater challenge with our final two periods of study, obtained during near encounters with the moon Callisto. Figure 12 provides observations of the C9 Callisto encounter (day 176, 1997). The distance to Callisto's center is shown in Figure 12a (bottom) in units of Callisto radii. In a Callisto-centered coordinate system, Galileo follows a path that is roughly parallel to the vector that points from Callisto to Jupiter and passes upstream of Callisto with respect to the corotating magnetospheric plasmas. A region of modest magnetic field pileup (20–30% over background), as diagnosed with Galileo's magnetometer instrument [*Kivelson et al.*, 1999] is shown just above Figure 12a (bottom).

[30] The beam and cigar distributions on the extreme left of Figure 12a clearly are unrelated to the immediate Callisto environment. More structured beaming occurs very close to Callisto and also some distance from Callisto, as shown on the extreme right of Figure 12a. The degree to which the immediate Callisto environment itself is responsible for the nearest-to-Callisto beams cannot be ascertained, but, clearly, structured beaming occurs elsewhere as well. Figure 12b shows examples of the beaming that is observed.

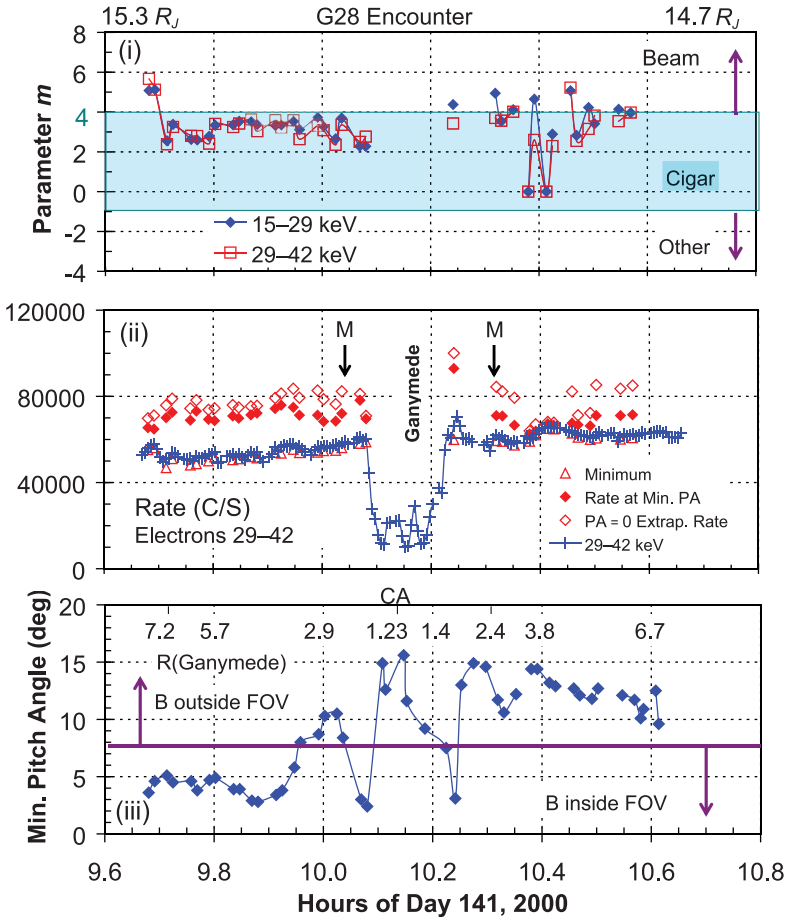

Figure 11a. Results of fitting the pitch-angle distributions for a high-resolution sample period designated as the G28 Encounter period. The description is the same as in the Figure 9a legend.

[31] Our final high time-resolution period (Orbit C3 on day 309, 1996) is shown in Figure 13, where we suspect that the moon Callisto may have had a profound effect on the beaming characteristics of the pitch-angle distributions. In this case, Galileo passed into the plasma wake of Callisto; the green bar above Figure 13a (bottom) shows when Galileo resided within the geometric wake (radial distances to Callisto are shown in the Figure 13a (bottom)). Outside of the geometric wake we see no beams. Examples of the rather dramatic beams observed are shown in Figure 13b. This encounter is reminiscent of the Io wake encounter in 1995 [*Williams et al.*, 1996] where, as described in section 1, electron beams were observed in Io's wake. We suspect that, as with Io, these Callisto beams are generated by an auroral current circuit stimulated by the motion of Jupiter's magnetized plasmas over and past the obstacle represented by Callisto's conducting ionosphere [*Kliore et al.*, 2002]. However, because electron beams can be observed elsewhere in Callisto's broader environment irrespective of Callisto's immediate presence (Figure 9), the beams observed in Callisto's wake could have been generated by Jupiter irrespective of Callisto's presence. The beams observed in Callisto's wake may have been there simply by happenstance. The C3 encounter with Callisto, and the possibility that that the Callisto interaction is responsible for the observed beams, will be examined in detail in a future paper.

5. Spectral Properties

[32] The beams documented in Figures 9a–13b are characterized roughly with a power-law energy distribution above the ~15-keV minimum energy observed (Figure 14). In this respect, they are consistent with the distributions observed in Io's wake [*Mauk et al.*, 2001] and in Saturn's middle magnetosphere [*Saur et al.*, 2006]. While the <25-keV portions of the Earth magnetospheric beams characterized by *Klumpar et al.* [1988] are not well-characterized with a power-law distribution shape [see *Mauk et al.*, 2001, Figure 7], the beams nonetheless are broadly distributed in energy and lack any distinct feature in their energy distributions. For the spectra shown in Figure 14, the power-law spectral indices (γ in the expression: $I \sim E^{-\gamma}$, where E is energy) are roughly $\gamma \sim 2.5$. This value is the same as some of the spectral indices reported by *Saur et al.* [2006] for Saturn and is consistent with the electron beam spectrum from Io's plasma tail reported by *Mauk et al.* [2001].

[33] *Frank and Paterson* [2002, 2004] have reported observing at lower energies some intensity versus energy distributions in Jupiter's middle magnetosphere with local

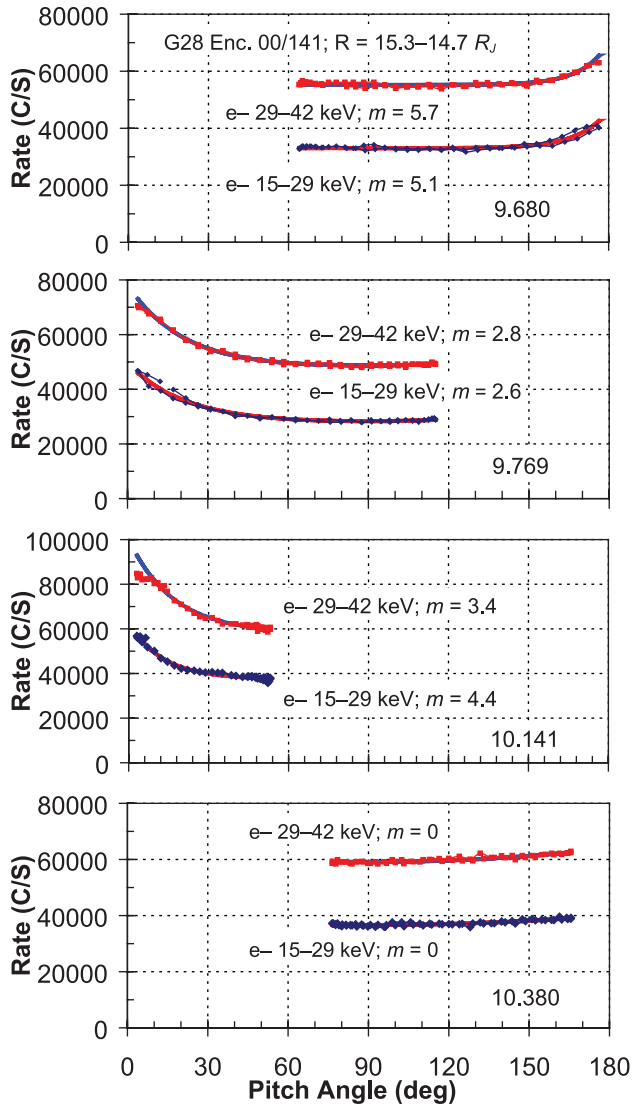

Figure 11b. Sample electron pitch-angle distributions and fits selected from the time period represented in Figure 11a.

peaks in the approximately kiloelectronvolt energy range. The PSD versus energy distributions are, however, monotonic (W. R. Paterson, private communication, 2007). Are these distributions, perhaps along with the higher-energy tails reported here, more closely related to the injection-stimulated electron beams reported by *McIlwain* [1975] (our Figure 3, with the peaked PSD energy distributions) than they are to the Klumpar-Carlson beams closely associated with the electric circuit that participates with the generation of the main ring of discrete aurora? The short answer is that we do not know.

[34] The long answer takes into account the fact that some injection phenomena have been studied at Jupiter and that the radial distribution of injections is not consistent with the distribution of beaming characteristics [*Mauk et al.*, 1999, Figure 13]. Our alternative interpretation takes account of the discussions by *Ergun et al.* [1998] that note that the upward accelerated electron beams associated with downward currents represent a mixture of coherent and stochastic acceleration. For example, the average energy of the accelerated distributions is correlated closely with the low-altitude electrostatic potential through which the electrons propagate. On the other hand, the high-energy tails of the distributions extend at least an order of magnitude in energy higher than that electrostatic potential drop. We hypothesize that the balance between coherent and stochastic acceleration can be different at Jupiter than it is at Earth. A third possibility is that *Frank and Paterson* [2002, 2004] are right and that, contrary to what happens at Earth, these beams are directly, rather than indirectly as we propose, associated with the generation of the discrete auroral emissions within the main auroral ring of Jupiter.

6. Magnetic Signatures of Electric Current

[35] If the bidirectional electron beams are generated by field-parallel electric currents connecting Jupiter with its space environment, then one might expect that structuring within the beaming characteristics should be reflected within magnetic signatures of the electric currents. *Saur et al.* [2002, 2006] have demonstrated that the magnetic field in Jupiter's middle magnetosphere is not quiet but includes magnetic field perturbations on various spatial/temporal scales. The authors show that these fluctuating fields can be described as weak turbulence, i.e., a bath of weakly nonlinearly interacting Alfvén waves. The amplitude of the fluctuations, and thus the turbulence power distribution, maximizes in the regions that map to Jupiter's most intense aurora. This finding is consistent with the idea that turbulent Alfvén waves exchange energy between the magnetosphere and the auroral ionosphere. Such turbulent fields are observed in the general region of electron bidirectional beaming, as displayed in Figure 15.

[36] It is impossible to uniquely relate magnetic field fluctuations like those shown in Figure 15 to field-aligned currents based on the time series measurement of a single spacecraft, i.e., in this case Galileo. However, by making simplifying assumptions an estimate of the relationship can be obtained. For an estimate, we rotate the data to a coordinate system in which z is along the background magnetic field. The coordinate x lies in the plane spanned by the magnetic field vector **B** and the direction of rotation of the spin equator and is perpendicular to the z direction. The coordinate y completes a right-hand coordinate system. The background field also is removed, and large-scale trends are removed from the data. The electric current is given by the curl of the magnetic field. On the temporal scale of concern, we can neglect Maxwell's displacement current. The field-aligned current is given by $J_{\|} = 1/\mu_0\,(\partial B_y/\partial x - \partial B_x/\partial y)$. We do not have both derivatives available to calculate $J_{\|}$. If we assume that one component of **B** is representative of $J_{\|}$ and that the temporal scales predominantly are spatial, then we can rewrite $J_{\|} = v_0/\mu_0\ \partial B_y/\partial t$. The velocity v_0, roughly in the x direction, is the relative velocity between the spacecraft and the plasma carrying the magnetic field. The results for $J_{\|}$ are shown in Figure 16, where we assumed $v_0 = 100$ km/s.

[37] The electric current estimate in Figure 16 shows strong structuring, as expected from Figure 15. Structures that are 1–2 min wide correspond to spatial scales that are 0.1–0.2 R_J given the 100 km/s rotational velocity. The

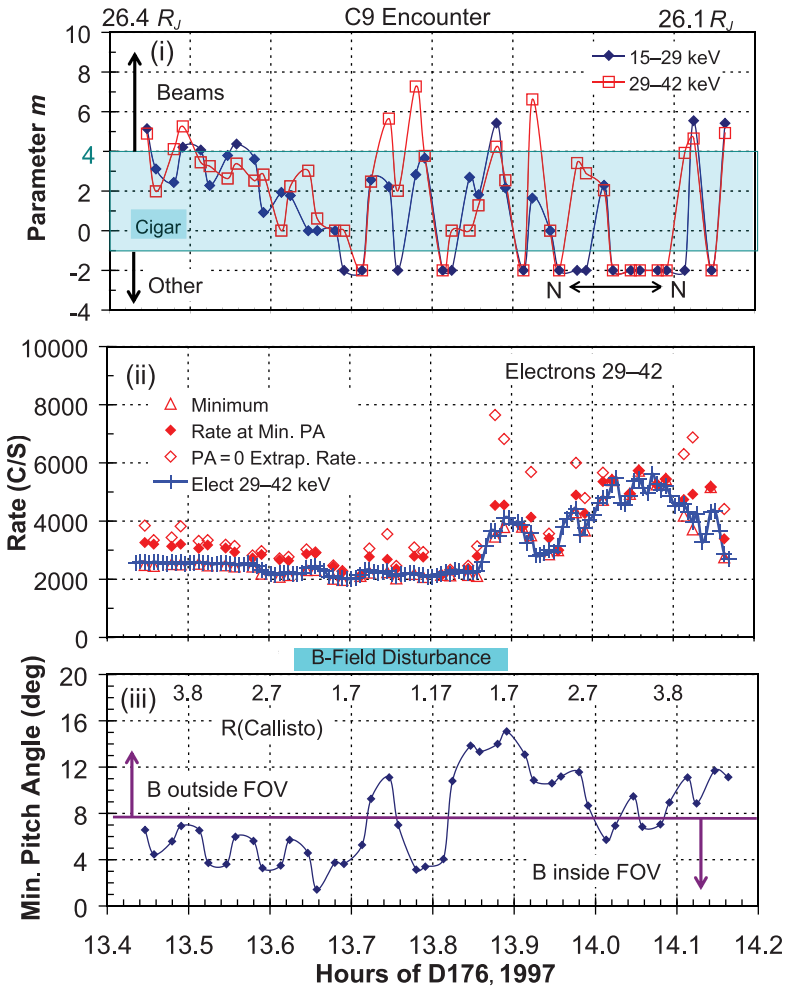

Figure 12a. Results of fitting the pitch-angle distributions for a high-resolution sample period designated as the C9 Encounter period. The description is the same as in the Figure 9a legend.

large-scale magnetospheric electric current densities diagrammed in Figure 5 have magnitudes of the order $\sim 2 \times 10^{-12}$ A/m^2 [*Khurana*, 2001] or from $\sim 2 \times 10^{-12}$ A/m^2 to $\sim 2 \times 10^{-11}$ A/m^2 [*Gustin et al.*, 2004]. Our estimates in Figure 16 render current densities up to a factor of 100 larger. To the extent that some fraction of our estimate represents true currents, after relaxation of our simplifying assumptions, these currents easily could sit on top of the large-scale upward going current system and locally reverse the direction of the electric current. On those field lines with the reversed electric current, we then expect antiplanetward electron beams to be created when the currents are sufficiently strong to be in a charge-carrier-limited condition at the low-altitude acceleration regions.

[38] While the results of this section show that structuring within the magnetic field generally is present, the details of that magnetic field structuring do not correlate directly with the details of the electron beam structuring for the specific beam-like distributions shown in Figures 9–13, i.e., the locations of peaks in estimated currents and those of the electron beams do not exactly coincide. Detailed correlation is not expected given Alfvénic-scale time delays between our observation positions and the auroral ionosphere. We also will argue in the next section that the beams that we have seen with our very limited sampling perhaps were not actively being generated at the time that they were observed. While the most distinct beams undoubtedly demarcate the positions of relatively recent beam generation, the beams when observed were likely in various stages of decay.

[39] While the high-energy electron components studied in this paper generally are not thought to carry the predominant auroral electric currents, it is nonetheless interesting to consider how much current might be carried by them. By integrating a mean of the $R \sim 25$–26 R_J spectra shown in Figure 14 [$I \sim 10^5$ $(E_{keV}/10)^{-2.5}$ cm^{-2} s^{-1} sr^{-1} keV^{-1}] along one of the two directions of the bidirectional electron beams and including only those electrons that reside within the loss cone, one obtains the current density entering or leaving the auroral zone at atmospheric altitudes equal to ~ 0.003 μA/m^2 for E > 10 keV and 0.1 μA/m^2 for E > 1 keV (spectrum extrapolated). A similar calculation for the $R \sim 18$ R_J spectra (data not shown) yields E > 10 keV and E > 1 keV (extrapolated) current densities of 0.015 μA/m^2 and 0.4 μA/m^2, respectively. Currents associated with strong Jovian auroral emissions are estimated at 0.04–0.4 μA/m^2 [*Gustin et al.*, 2004], which is not outrageously different from

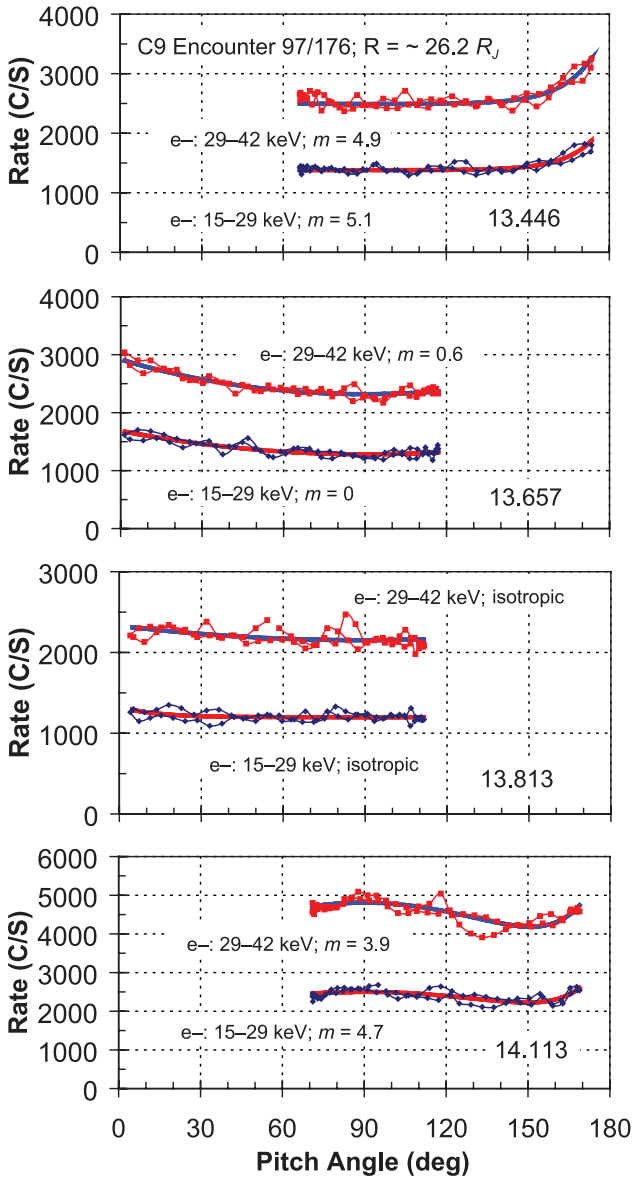

Figure 12b. Sample electron pitch-angle distributions and fits selected from the time period represented in Figure 12a. (bottom) Shown is an example in which the beam-like characteristic only marginally satisfies our statistical test.

the potential values given here for our beams. However, the beams are thought to be accelerated upward rather than downward, and they occur in regions absent of auroral emissions [*Carlson et al.*, 1998]. So, the relevance of these current calculations is unclear.

7. Discussion

[40] It is our expectation that, although the source of power for auroral activity is very different at Jupiter than it is at Earth, the physical processes for these two systems are closely analogous. For the equatorial electron beam phenomena addressed here, that expectation along with the evidence presented here leads to the interpretation presented in Figure 17 (upper and lower). Specifically, within the broad region of generally upward (away from Jupiter) magnetic field-aligned currents that map generally to Jupiter's bright oval of discrete aurora, the electric currents are highly structured with regions of strong downward currents closely adjacent to regions of strong upward currents. Such current structures may be spatial in character, but they could relate to turbulent Alfvén waves [e.g., *Saur et al.*, 2002, 2006]. Single spacecraft observations, however, do not provide the possibility to distinguish if the nature of the structuring is spatial or temporal or a mixture of both of them. Presumably, the net current represented by an integral across this broad region still would yield net upward current and would therefore be broadly self-consistent with the forces needed to maintain partial corotation of plasmas radially transported outward from the Io torus source region (Figure 17, lower). With this interpretation, bright discrete aurora would be generated in regions of strong upward current, whereas our bidirectional equatorial electron beams would be generated in the regions of strong downward current. Once generated, the electron beams in various stages of evolution and transport would become a regular component of the plasma populations of the middle equatorial magnetosphere, explaining perhaps the persistence of the field-aligned enhancements in the middle magnetosphere documented by *Tomás et al.* [2004a, 2004b]. Also, as this component evolves and is transported to other regions, it also may become a source population for other components of Jupiter's aurora, specifically as postulated by *Tomás et al.* [2004a, 2004b], the source of the diffuse aurora that extends equatorward of the oval of bright discrete aurora.

[41] How does the interpretation in Figure 17 stand up to the evidence presented here? The prime evidence presented here is the spatial/temporal structuring of the equatorial electron beams. This structuring has been established by quantifying the qualitative "notion" of the electron beaming into a numerical parameter and then examining the behavior of that parameter in high-time resolution. We find that even within the confines of time periods of roughly <1 to 2 hours, with Galileo moving distances of only 0.3 to <1 R_J, a variety of angular distribution shapes typically are observed (isotropic, cigar, beaming), and the beaming characteristics can come and go on a time scale of several minutes. If we assume that the structures are spatial in character, the spatial scales estimated at auroral altitudes range from <20 km (several minute features at Galileo) to ~300 km.

[42] The >15-keV energy spectra of the beams are broad with power-law-like distributions, suggesting that stochastic processes are responsible for the energization. This characteristic (broad, featureless distributions) is in accordance with the character of the equatorial electron beams discovered by *Klumpar et al.* [1988] and interpreted by *Carlson et al.* [1998] as being generated at low altitudes on auroral field lines that carry downward currents. On the other hand, low-energy spectra associated with beams at times show intensity spectra with local maxima in the kiloelectronvolt energy range [*Frank and Paterson*, 2002, 2004]. While peaked spectra of electron beams are observed in Earth's equatorial magnetosphere in association with transient magnetic field-aligned currents that accompany dynamic injec-

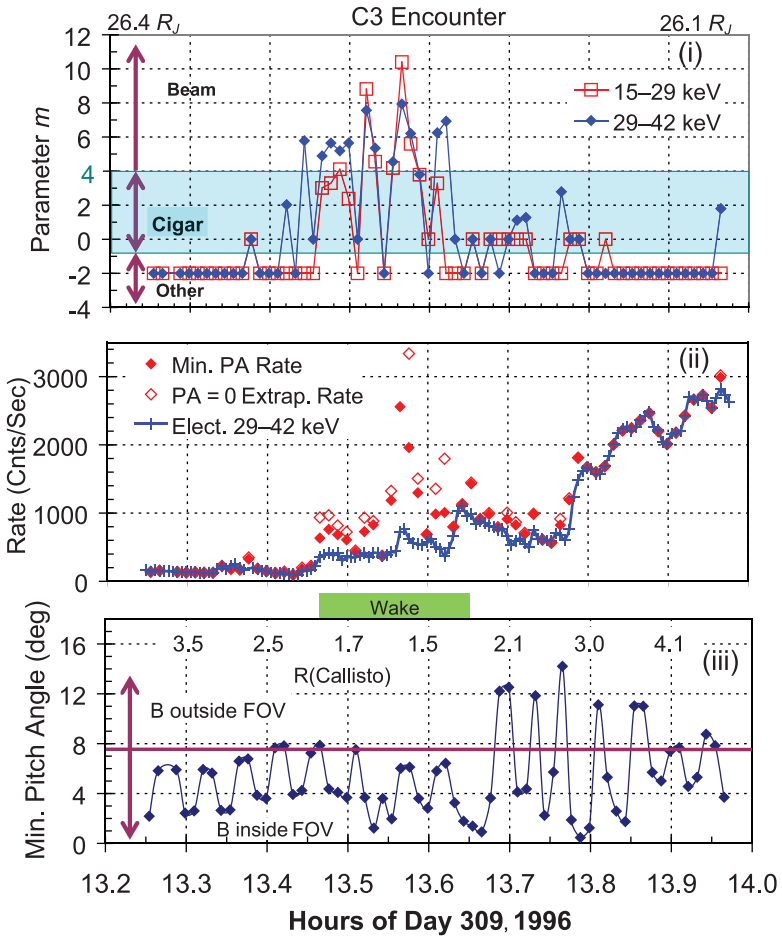

Figure 13a. Results of fitting the pitch-angle distributions for a high-resolution sample period designated as the C3 Encounter period. The description is the same as in the Figure 9a legend.

tion phenomena (Figure 3), they represent phenomena that appear distinct from the Klumpar-Carlson beams thought to accompany the main oval of Earth's discrete aurora. The dynamic injections at Jupiter that could explain peaked intensity features within the equatorial electron beams using Earth-like processes appear to have a radial profile of occurrence [*Mauk et al.*, 1999] that is very different than the radial profile of electron beam occurrence [*Tomás et al.*, 2004a, 2004b]. It is possible that *Frank and Paterson* [2002, 2004] are correct in asserting that these beams are associated directly with the generation of discrete aurora at Jupiter in a fashion that is not anticipated from Earth's auroral processes. However, *Ergun et al.* [1998] show that the energization of the upward accelerated Klumpar-Carlson beams has contributions from both coherent and stochastic processes. In keeping with our hypothesis as represented by Figure 17, it is our assumption that the signatures of coherent acceleration at times are maintained within the upward accelerated electron beams at Jupiter in a fashion that has not been identified at Earth.

[43] Our analysis shows that the magnetic field within the regions that show the field-aligned electron beams is highly structured in a fashion that in part could represent field-aligned current structures as sketched in Figure 17. However, as previously acknowledged, we find no one-to-one correlation between the electron beam structures that we observed and the signatures of magnetic field-aligned currents that we have estimated with simplifying assumptions. However, a detailed correlation is not expected given Alfvénic-scale time delays between our observation point and the auroral ionosphere. We also believe that the beams that we observed were not necessarily being generated at the times that they were observed. The most distinct beams are, we believe, remnants of beams that were generated in time periods that are relatively recent with respect to the observation times. This statement begs the question of what a beam would look like if it actively were being generated. Figure 18 shows a hint of an answer. It shows a fit of one beam reported by *Klumpar et al.* [1988] and shown in Figure 1 (left). The fitting parameter has a value of $m \sim 21$, which is a factor of 2 higher than any persistent beams that we have observed in Jupiter's middle magnetosphere.

[44] It also is of interest to consider the maximum width that the beams would have if they were generated at auroral acceleration altitudes and propagated to the observation point without scattering. The beams would achieve their maximum widths with this scenario if the energization process acted on the electron distributions isotropically. If the distributions are generated at an altitude of 1 R_J, with field strength of roughly 50 μT, the beams would have

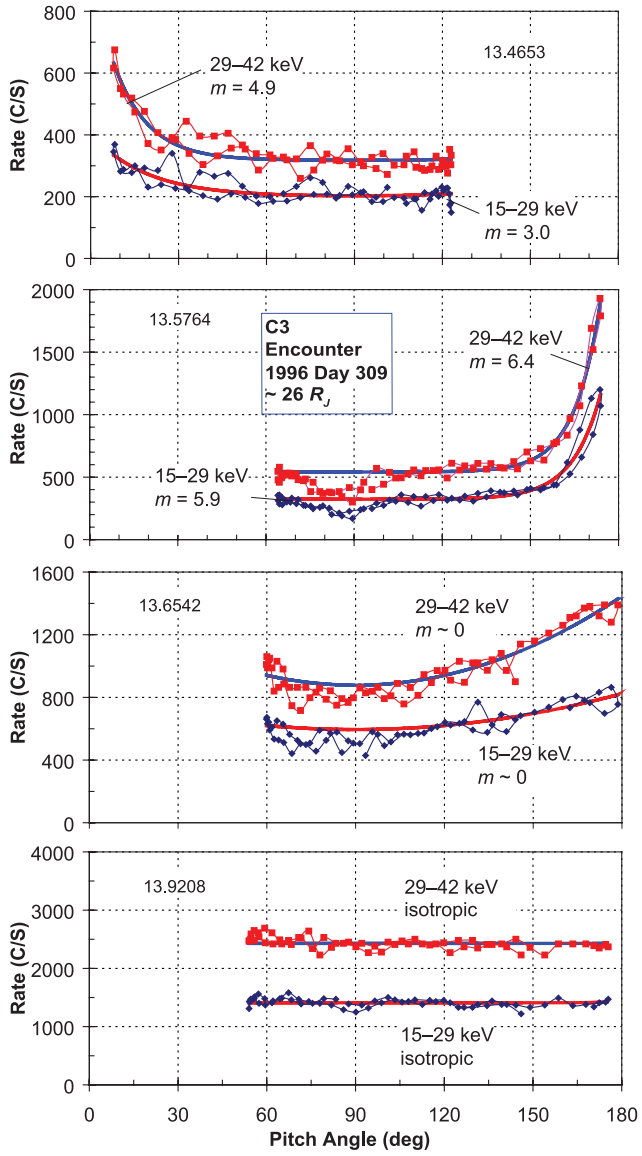

Figure 13b. Sample electron pitch-angle distributions and fits selected from the time period represented in Figure 13a.

widths near the equator at 20 R_J (B ~ 20 nT) of a degree or so, with m values much higher than 21. For the Earth case revealed by *Klumpar et al.* [1988], a similar calculation yields a beam width of ~2 degrees, a value roughly commensurate with the m value of 21 above. To the extent that our hypothesis for Jupiter has validity, angular scattering must be involved between the time that the beams are generated and the time that they are observed.

[45] A possible reason that such distinct beams with high values of m were not observed with Galileo EPD within Jupiter's middle magnetosphere is the scarcity of high time-resolution data. It may be difficult to see beams that actively are being generated with such sparse and random samples. On the other hand, the m value for the Io beam in Figure 1 right, which must have been generated within the time that it takes the plasmas to flow the short distance from Io to the measurement point, some 0.5 Io radii from Io, is of order ~10, again roughly a factor of 2 below the value for the *Klumpar et al.* [1988] beams. We do know that, at least at times, the scattering can be very rapid. For example, with distributions observed over Ganymede's pole on field lines connected directly to Ganymede, it was possible to determine that strong scattering, to the extent of generating isotropic distributions, was occurring within the time period of a single bounce [*Williams and Mauk*, 1997; *Williams et al.*, 1998]. Thus ascertaining the age of the observed beams in Jupiter's middle magnetosphere is very difficult.

[46] A final topic worthy of discussion is the observation of electron beams in Callisto's wake that potentially are generated by the Callisto–magnetosphere interaction. Such a discussion awaits the more detailed analyses to be presented in a future paper.

8. Conclusions

[47] While the discussions here make it apparent that we cannot be definitive in explaining all details of our observations, certain things are clear. The observed equatorial electron beams are structured down to observations time of less than several minutes, corresponding to auroral scale size of <20 km if the structures are assumed to be spatial in character. In the same regions of the beam observations, we see structured magnetic field fluctuations likely associated with structured currents. These magnetic field fluctuations are consistent with turbulent Alfvén waves maximizing in

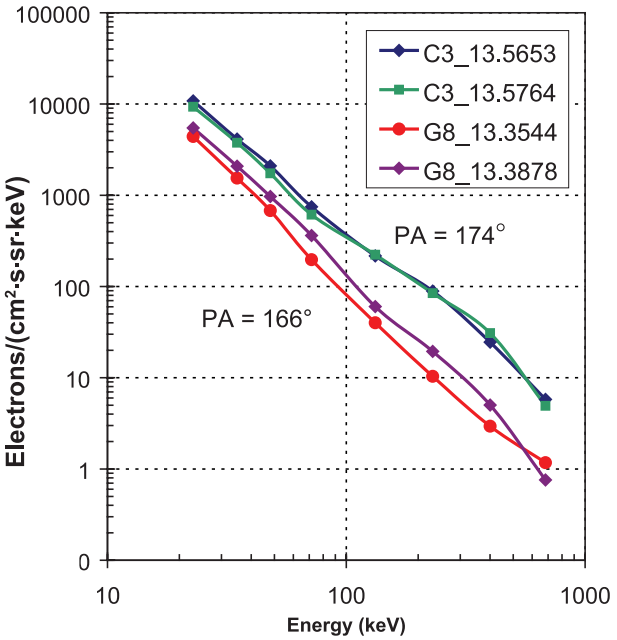

Figure 14. Intensity versus energy spectra sampled near 25 R_J from the G8 Plasma Sheet period shown in Figure 9 (sampled far away from any icy moon) and sampled near 26 R_J from the C3 Encounter period shown in Figure 13. The C3 Encounter data spectra were obtained within the plasma wake of Callisto. Straight lines on these log–log plots represent power-law distributions. The power spectral indices (γ in the expression $I \sim E^{-\gamma}$, where E is energy) is roughly $\gamma \sim 2.5$.

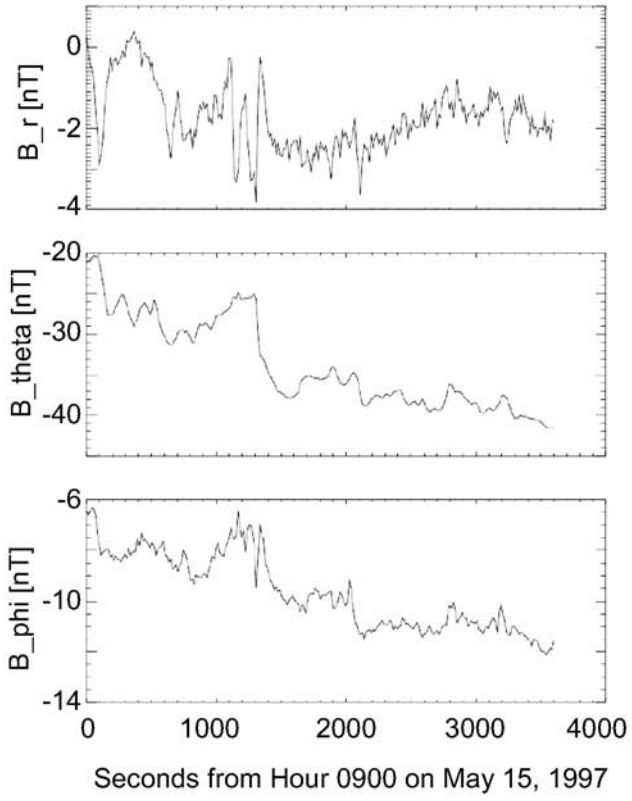

Figure 15. Galileo spacecraft magnetic field data with temporal resolution of 14 s. This subset of 1 hour of data is from orbit g08, 15 May 1997, starting at 0900, and at a radial distance of 24.8 R_J. The coordinate system is a spherical system fixed to and aligned with Jupiter's planetary spin system.

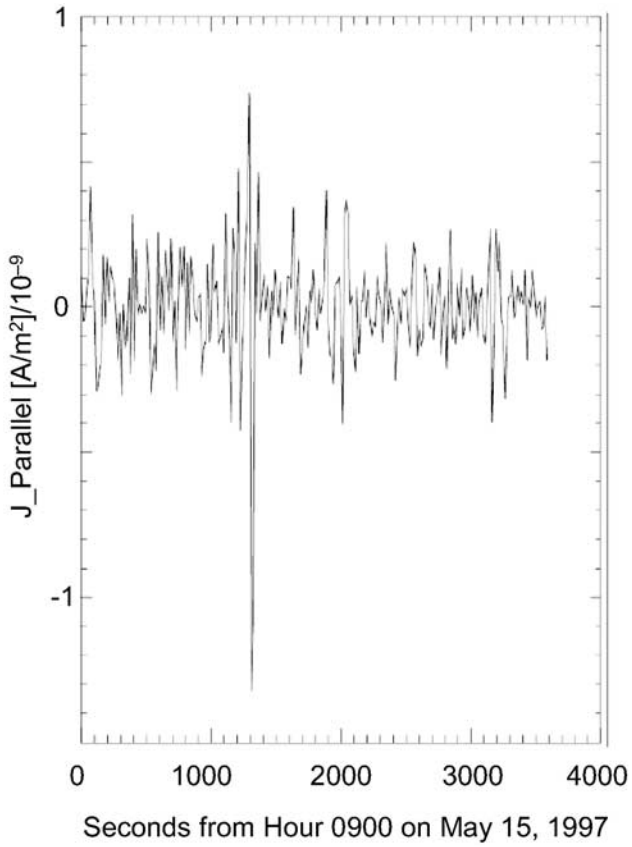

Figure 16. Temporal derivative (see text) of the magnetic field as a rough proxy for the electric current along the background magnetic field for the time interval shown Figure 15.

the same region [*Saur et al.*, 2002]. The beams are observed in regions that map magnetically to Jupiter's strong auroral regions and are similar to beams observed within Earth's equatorial magnetosphere that map magnetically to Earth's strong auroral regions. Because it has been demonstrated that Earth's beams are generated at low altitudes within regions of downward auroral electric currents, and because of the similarities between the Earth's and Jupiter's beams mentioned above, we conclude that the Jupiter beams likely are generated at low altitudes within regions of downward auroral electric currents. Because the beams at Jupiter are highly structured and because strong aurora are expected in regions of upward auroral currents, we also conclude that the auroral field-aligned currents at Jupiter likely are structured like they are at Earth, with regions of downward currents closely adjacent to regions of upward currents. The magnetosphere–ionosphere coupling likely is more structured and perhaps dynamic than previous large-scale models would suggest [*Cowley and Bunce*, 2001; *Hill*, 2001], as suggested by *Dougherty et al.* [1998]. A spatial-temporal averaging of our picture, however, would be qualitatively consistent with previous large-scale models (Figure 17, lower).

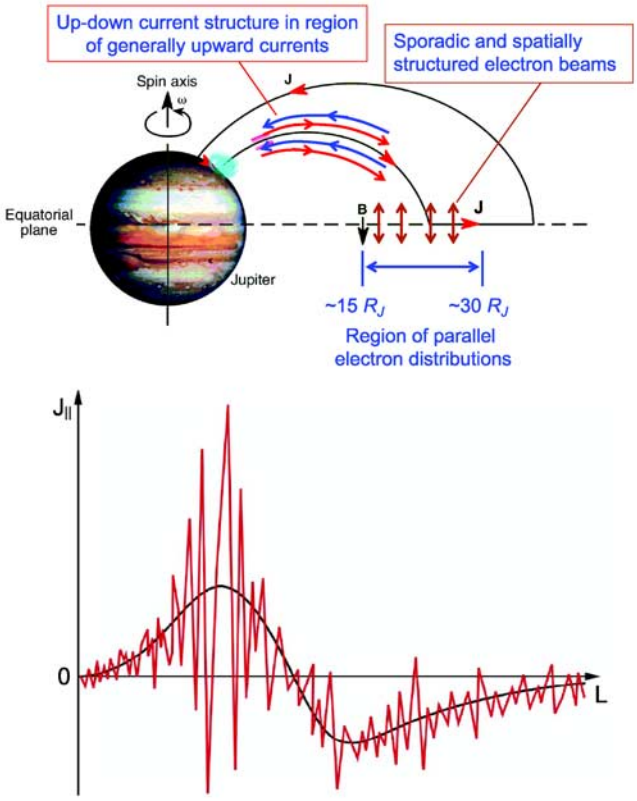

Figure 17. (top) A reinterpretation of the concept shown in Figure 5. The data presented here indicate that the electron beams are spatially structured. On the basis of our Earth-derived assumption that such beams are generated in regions of downward (with respect to Jupiter) electric currents, this finding implies that the auroral currents themselves are highly structured with a pattern of strong upward and downward currents embedded in the broad region that on average is a region of generally upward currents. (bottom) Notional sketch of field-aligned electric currents as a function of radial distance. The red line shows a highly structured electric current system that we infer in this paper. We expect a spatial and temporal average of these currents (black curve) to render the static magnetosphere–ionosphere coupling currents derived by *Hill* [1979, 2001] and *Cowley and Bunce* [2001].

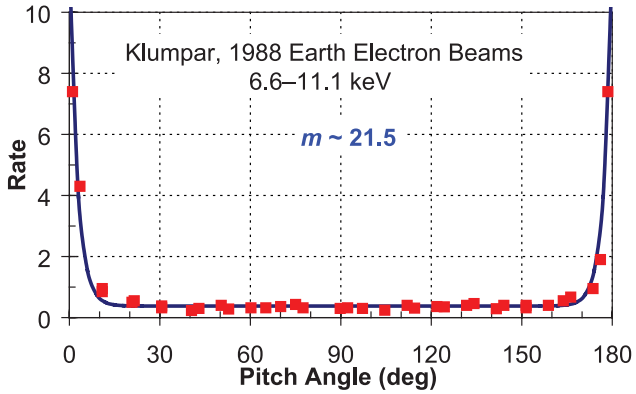

Figure 18. A replotting and fitting of the Earth-observed electron beam data published by *Klumpar et al.* [1988] and shown in our Figure 1 (left). The high value of *m* obtained may more closely represent values expected while the beams actively are being generated and before the beams are degraded over time by scattering.

[48] A key open question concerns the mechanisms of upward field-aligned acceleration. We propose that differences in the details of the broad upward-accelerated spectra observed in both the Earth and Jupiter systems may correspond to differences in the relative importance of the contributions of coherent and stochastic acceleration processes. Both kinds of processes appear to contribute to the acceleration at both Jupiter and Earth.

[49] **Acknowledgments.** We thank Sven Jacobsen of the Institut für Geophysik und Meteorologie Universität zu Köln for preparing Figure 17, lower. Magnetic field data in Figures 15 and 16 kindly were provided by M. G. Kivelson, the principal investigator of the Galileo magnetometer experiment. Funding for this research was provided by National Space and Aeronautics Administration (NASA) grants from the Outer Planets Research Program and from the Geospace Research Program.

[50] Wolfgang Baumjohann thanks Richard Thorne and another reviewer for their assistance in evaluating this paper.

References

Anderson, L., et al. (2002), Characteristics of parallel electric fields in the downward current region of the aurora, *Phys. Plasmas*, *9*, 3600–3609.

Bhattacharya, B., R. M. Thorne, and D. J. Williams (2001), On the energy source for diffuse Jovian auroral emissivity, *Geophys. Res. Lett.*, *28*, 2751–2754.

Carlson, C. W., et al. (1998), FAST observations in the downward auroral current regions: Energetic upgoing electron beams, parallel potential drops, and ion heating, *Geophys. Res. Lett.*, *25*, 2017–2020.

Cowley, S. W. H., and E. J. Bunce (2001), Origin of the main auroral oval in Jupiter's coupled magnetosphere-ionosphere system, *Planet. Space Sci.*, *49*, 1067–1088.

Dougherty, M. K., M. W. Dunlop, R. Prange, and D. Rego (1998), Correspondence between field aligned currents observed by Ulysses and HST auroral emissions, *Planet. Space Sci.*, *46*, 531–540.

Ergun, R. E., et al. (1998), FAST satellite observations of electric field structures in the auroral zone, *Geophys. Res. Lett.*, *25*, 2025–2028.

Frank, L. A., and W. R. Paterson (1999), Intense electron beams observed at Io with the Galileo spacecraft, *J. Geophys. Res.*, *104*, 28,657–28,670.

Frank, L. A., and W. R. Paterson (2000), Observations of plasmas in the Io torus with the Galileo spacecraft, *J. Geophys. Res.*, *105*, 16,017–16,034.

Frank, L. A., and W. R. Paterson (2002), Galileo observations of electron beams and thermal ions in Jupiter's magnetosphere and their relationship to auroras, *J. Geophys. Res.*, *107*(A12), 1478, doi:10.1029/2001JA009150.

Frank, L. A., and W. R. Paterson (2004), Plasmas observed near local noon in Jupiter's magnetosphere with the Galileo spacecraft, *J. Geophys. Res.*, *109*, A11217, doi:10.1029/2002JA009795.

Fritz, T. A., et al. (1977), Significant initial results from the environmental measurements experiment on ATS-6, *Tech. Pap. 1101*, NASA Sci. and Tech. Inf. Off., Washington, D. C.

Gustin, J., et al. (2004), Energy-flux relationship in the FUV Jovian aurora deduced from HSTSTIS spectral observations, *J. Geophys. Res.*, *109*, A10205, doi:10.1029/2003JA010365.

Hill, T. W. (1979), Inertial limit on rotation, *J. Geophys. Res.*, *84*, 6554–6558.

Hill, T. W. (2001), The Jovian auroral oval, *J. Geophys. Res.*, *106*, 8101–8108.

Khurana, K. K. (2001), Influence of solar wind on Jupiter's magnetosphere deduced from currents in the equatorial plane, *J. Geophys. Res.*, *106*, 25,999–26,016.

Kivelson, M. G., K. K. Khurana, D. J. Stevenson, L. Bennet, S. Joy, C. T. Russell, R. J. Walker, C. Zimmerman, and C. Polanskey (1999), Europa and Callisto: Induced or intrinsic fields in a periodically varying plasma environment, *J. Geophys. Res.*, *104*, 4609–4626.

Kliore, A. J., A. Anabtawi, R. G. Herrera, S. W. Asmar, A. F. Nagy, D. P. Hinson, and F. M. Flasar (2002), Ionosphere of Callisto from Galileo radio occultation observations, *J. Geophys. Res.*, *107*(A11), 1407, doi:10.1029/2002JA009365.

Klumpar, D. M., J. M. Quinn, and E. G. Shelley (1988), Counter-streaming electrons at the geomagnetic equator near 9 R_E, *Geophys. Res. Lett.*, *15*, 1295–1298.

Lanzerotti, L. J., et al. (1993), Measurements of hot plasmas in the magnetosphere of Jupiter, *Planet. Space Sci.*, *41*, 893–917, doi:10.1016/0032-0633(93)90096-K.

Marklund, G., et al. (2001), Temporal evolution of the electric field accelerating electrons away from the auroral ionosphere, *Nature*, *414*, 724–727.

Mauk, B. H., and C.-I. Meng (1991), The aurora and middle magnetospheric processes, in *Auroral Physics*, edited by C.-I. Meng, M. J. Rycroft, and L. A. Frank, pp. 223–239, Cambridge Univ. Press, Cambridge, U. K.

Mauk, B. H., D. J. Williams, R. W. McEntire, K. K. Khurana, and J. G. Roederer (1999), Storm-like dynamics of Jupiter's inner and middle magnetosphere, *J. Geophys. Res.*, *104*, 22,759–22,778.

Mauk, B. H., D. J. Williams, and A. Eviatar (2001), Understanding Io's space environment interaction: Recent energetic electron measurements from Galileo, *J. Geophys. Res.*, *106*, 26,195–26,208.

Mauk, B. H., B. J. Anderson, and R. M. Thorne (2002), Magnetosphere-ionosphere coupling at Earth, Jupiter, and beyond, in *Atmospheres in the Solar System*, *Comparative Aeronomy*, *Geophys. Monogr. Ser.*, vol. 130, edited by M. Mendillo, pp. 97–114, AGU, Washington, D. C.

McIlwain, C. E. (1975), Auroral electron beams near the magnetic equator, in *The Physics of Hot Plasma in the Magnetosphere*, edited by B. Hultqvist and L. Stenflo, pp. 91–105, Plenum, New York.

Meng, C. I., M. J. Rycroft, and L. A. Frank (1991), *Auroral Physics*, Cambridge Univ. Press, Cambridge, U. K.

Nishida, A. (1976), Outward diffusion of energetic particles from the Jovian radiation belt, *J. Geophys. Res.*, *81*, 1771–1773.

Saur, J., H. Politano, A. Pouquet, and W. H. Matthaeus (2002), Evidence for weak MHD turbulence in the middle magnetosphere of Jupiter, *Astron. Astrophys.*, *386*, 699–708.

Saur, J., A. Pouquet, and W. H. Matthaeus (2003), An acceleration mechanism for the generation of the main auroral oval on Jupiter, *Geophys. Res. Lett.*, *30*(5), 1260, doi:10.1029/2002GL015761.

Saur, J., et al. (2006), Anti-planetward auroral electron beams at Saturn, *Nature*, *439*, 600–702, doi:10.1038/nature04401.

Su, Y.-J., R. E. Ergun, F. Bagenal, and P. A. Delamere (2003), Io-related Jovian auroral arcs: Modeling parallel electric fields, *J. Geophys. Res.*, *108*(A2), 1094, doi:10.1029/2002JA009247.

Temerin, M., and C. W. Carlson (1998), Current-voltage relationship in the downward auroral current region, *Geophys. Res. Lett.*, *25*, 2365–2368.

Tomás, A., J. Woch, N. Krupp, A. Lagg, K.-H. Glassmeier, and W. S. Kurth (2004a), Energetic electrons in the inner part of the Jovian magnetosphere and their relation to auroral emissions, *J. Geophys. Res.*, *109*, A06203, doi:10.1029/2004JA010405.

Tomás, A., J. Woch, N. Krupp, A. Lagg, K.-H. Glassmeier, M. K. Dougherty, and P. G. Hanlon (2004b), *Planet. Space Sci.*, *52*, 491–498, doi:10.1016/j.pss.2003.06.011.

Vasyliunas, V. M. (1983), Plasma distribution and flow, in *Physics of the Jovian Magnetosphere*, edited by A. J. Dessler, p. 395, Cambridge Univ. Press, Cambridge, U. K.

Williams, D. J. (2001), Ganymede's ionic radiation belts, *Geophys. Res. Lett.*, *28*, 3793–3796.

Williams, D. J., and B. H. Mauk (1997), Pitch-angle diffusion at Jupiter's moon Ganymede, *J. Geophys. Res.*, *102*, 24,283–24,287.

Williams, D. J., R. W. McEntire, S. Jaskulek, and B. Wilken (1992), The Galileo energetic particles detector, *Space Sci. Rev.*, *60*, 385–412.

Williams, D. J., et al. (1996), Electron beams and ion composition measured at Io and in its torus, *Science*, *274*, 401–403.

Williams, D. J., B. H. Mauk, and R. W. McEntire (1998), Properties of Ganymede's magnetosphere as revealed by energetic particle observations, *J. Geophys. Res.*, *103*, 17,523–17,534.

Williams, D. J., R. M. Thorne, and B. H. Mauk (1999), Energetic electron beams and trapped electrons at Io, *J. Geophys. Res.*, *104*, 14,739–14,754.

B. H. Mauk, Johns Hopkins University Applied Physics Laboratory, 11100 Johns Hopkins Road, Laurel, MD 20723, USA. (barry.mauk@jhuapl.edu)

J. Saur, Institut für Geophysik und Meteorologie, Universität zu Köln, Albertus-Magnus-Platz, D-50923 Köln, Germany. (saur@geo.uni-koeln.de)